Atmos. Chem. Phys. Discuss., 12, 29235–29288, 2012
www.atmos-chem-phys-discuss.net/12/29235/2012/
doi:10.5194/acpd-12-29235-2012

Atmospheric Chemistry and Physics Discussions

Regional CO_2 flux estimates for 2009–2010 based on GOSAT and ground-based CO_2 observations

S. Maksyutov[1], H. Takagi[1], V. K. Valsala[1,*], M. Saito[1,], T. Oda[1,***,****], T. Saeki[1], D. A. Belikov[1], R. Saito[1,*****], A. Ito[1], Y. Yoshida[1], I. Morino[1], O. Uchino[1], R. J. Andres[2], and T. Yokota[1]**

[1]National Institute for Environmental Studies, Tsukuba, Japan
[2]Oak Ridge National Laboratory, Oak Ridge, TN, USA
[*]now at: Indian Institute of Tropical Meteorology, Pune, India
[**]now at: Laboratoire des Sciences du Climat et l'Environnement, Gif sur Yvette, France
[***]now at: Colorado State University, Fort Collins, CO, USA
[****]now at: Global Monitoring Division, NOAA Earth System Research Laboratory, Boulder, CO, USA
[*****]now at: Japan Agency for Marine-Earth Science and Technology, Yokohama, Japan

Received: 31 July 2012 – Accepted: 9 October 2012 – Published: 13 November 2012

Correspondence to: S. Maksyutov (shamil@nies.go.jp)

Published by Copernicus Publications on behalf of the European Geosciences Union.

Abstract

We present the application of an integrated global carbon cycle modeling system to the estimation of monthly regional CO_2 fluxes from the column-averaged dry air mole fractions of CO_2 (X_{CO_2}) retrieved from the spectral observations made by the Greenhouse gases Observing SATellite (GOSAT). The regional flux estimates are to be publicly disseminated as the GOSAT Level 4 data product. The forward modeling components of the system include an atmospheric tracer transport model, an anthropogenic emissions inventory, a terrestrial biosphere exchange model, and an oceanic flux model. The atmospheric tracer transport was simulated using isentropic coordinates in the stratosphere and was tuned to reproduce the age of air. We used a fossil fuel emission inventory based on large point source data and observations of nighttime lights. The terrestrial biospheric model was optimized by fitting model parameters to match observed atmospheric CO_2 seasonal cycle, net primary production data, and a biomass distribution map. The oceanic surface pCO_2 distribution was estimated with a 4-D variational data assimilation system based on reanalyzed ocean currents. Monthly CO_2 fluxes of 64 sub-continental regions, between June 2009 and May 2010, were estimated from the GOSAT FTS SWIR Level 2 X_{CO_2} retrievals (ver. 02.00) gridded to $5^\circ \times 5^\circ$ cells and averaged on a monthly basis and monthly-mean GLOBALVIEW-CO2 surface-based observations. Our result indicated that adding the GOSAT X_{CO_2} retrievals to the GLOBALVIEW observations in the flux estimation would bring changes to fluxes of tropics and other remote regions where the surface-based observations are sparse. The uncertainty of these remote fluxes was reduced by as much as 60 % through such addition. For many of these regions, optimized fluxes are brought closer to the prior fluxes by the addition of GOSAT data. For the most of the regions and seasons considered here, the estimated fluxes fell within the range of natural flux variability estimated with the component models.

ACPD

12, 29235–29288, 2012

1 Introduction

The recent increase in atmospheric CO_2 concentration is partially abated by carbon uptake by ocean and land, which indicates disequilibrium in CO_2 exchanges between the atmosphere and oceans and between the atmosphere and the terrestrial biosphere (Keeling et al., 1995). The disequilibrium in the terrestrial carbon cycle can be attributed to the 20th century warming leading to enhanced nitrogen recycling in the biosphere coincident with an increase in CO_2 concentrations that facilitates photosynthesis and vegetation functioning (Melillo et al., 2002; Grant et al., 2009). The sustainability and amount of the terrestrial sink is still difficult to assess on large regional scales (e.g. Dolman et al., 2012; Gloor et al., 2012). The inverse modeling of carbon exchange at the Earth's surface plays important role in the quantification of the distribution of terrestrial carbon sinks. Analyses of the regional CO_2 fluxes using inverse models of atmospheric transport have proven useful for quantifying the spatial distribution and interannual variability of surface CO_2 fluxes on both global (Bousquet et al., 2000) and regional scales (Peters et al., 2007). One particularly important topic under investigation is the partitioning of the terrestrial carbon sink between (1) mid and high latitude regions of the Northern Hemisphere, where the warming is most pronounced (Jones and Briffa, 1992), and (2) wet tropical and subtropical regions, such as in southern China forests, where net ecosystem production is high (Piao et al., 2009). It was initially found that latitudinal CO_2 gradient suggested stronger Northern Hemisphere sinks (Tans et al., 1990). A more detailed analysis with atmospheric transport and inversion models allocated a large sink to the US (Fan et al., 1998), supported by a bottom-up estimate (Pacala et al., 2001). Later, the US sink estimate was reduced in a multi-model inverse modeling study (Gurney et al., 2002) where a significant net tropical source was also projected. Based on inverse model estimates of the vertical CO_2 gradients, Stephens et al. (2007) supported more moderate estimates of Northern Hemisphere extratropical sinks and near-neutral net CO_2 fluxes in the tropics. However, on a global scale, many gaps appear in remote areas that are not covered by conventional atmospheric CO_2

ACPD
12, 29235–29288, 2012

observation networks (mostly tropical regions), leaving space for large uncertainties in the reconstructed fluxes (Gloor et al., 2000). Rayner and O'Brien (2001) suggested an unconventional solution to the problem of data gaps, arguing that a large number of relatively low-precision satellite observations of atmospheric CO_2 concentration can be used to fill those gaps. This suggestion raised high expectations for the usefulness of remote sensing observations of atmospheric CO_2.

The launch of the Greenhouse gases Observing SATellite (GOSAT) in 2009, which observes high-resolution spectra of reflected light (Kuze et al., 2009), was followed by continuous efforts to refine retrievals of CO_2 and CH_4 column abundances (Yokota et al., 2009; Bösch et al., 2011; Butz et al., 2011; Yoshida et al., 2011; O'Dell et al., 2012; Oshchepkov et al., 2012). The availability of the GOSAT retrievals validated with Fourier Transform Spectrometer (FTS) observations collected in Total Carbon Column Observing Network (TCCON) (Morino et al., 2011) provides the scientific community with an opportunity to apply the newly available GOSAT data to carbon cycle studies. Theoretical studies on the utility of GOSAT observations by Chevallier et al. (2009), Kadygrov et al. (2009), and others suggested that the GOSAT data can help fill the observation network gaps if sufficient retrieval accuracy and precision are achieved.

This paper provides an overview of a carbon cycle modeling system that includes components for modeling atmospheric transport, anthropogenic CO_2 emissions, and terrestrial and oceanic CO_2 exchange; it further describes the application of the system to the estimation of surface CO_2 fluxes using the GOSAT observations. The components of the carbon cycle modeling system were developed specifically for processing the GOSAT data, aiming at the capability of utilizing early availability of the GOSAT observations for inverse model analysis with a delay of a year or less.

In our study, we assessed the utility of the GOSAT observations for inverse modeling of surface sources and sinks. We used a recently-improved version of GOSAT X_{CO_2} retrievals (version 02.00; Yoshida et al., 2013) and the GLOBALVIEW-CO2 ground-based observations (2011, hereafter denoted as GV). We estimated monthly regional fluxes and their uncertainties from (1) the ground-based GV data and (2) both GV

ACPD
12, 29235–29288, 2012

and GOSAT X_{CO_2} retrievals, and compare these two sets of results. The present study used GOSAT observations obtained during a one-year period between June 2009 and July 2010, the first year of GOSAT sounding. The results presented in the sections to follow are based on the latest version of the GOSAT Level 2 X_{CO_2} data product (ver. 02.00). Section 2 introduces the components of the modeling system. Section 3 briefly describes the GOSAT observations and the inverse model. Section 4 presents the results, and Sect. 5 concludes the paper.

2 Inverse modeling system components

In this section, we present the inverse modeling system components, including the component models for simulating atmospheric transport of the CO_2 by winds, the CO_2 exchange between the atmosphere and oceans and between the atmosphere and terrestrial biosphere, and emissions of CO_2 by fossil fuel consumption and cement manufacturing. The a priori flux dataset used here is comprised of four components: daily net ecosystem exchange (NEE), predicted by the terrestrial biosphere process model VISIT (Vegetation Integrative SImulator for Trace gases) (Ito, 2010; M. Saito et al., 2011); monthly ocean-atmosphere CO_2 fluxes generated by an ocean pCO_2 data assimilation system (Valsala and Maksyutov, 2010); monthly CO_2 emissions due to biomass burning, stored in the Global Fire Emissions Database (GFED), version 3.1 (van der Werf et al., 2010); and monthly fossil fuel CO_2 emissions obtained via combining the high-resolution Open source Data Inventory of Anthropogenic CO_2 emission (ODIAC) dataset (Oda and Maksyutov, 2011) and the Carbon Dioxide Information Analysis Center's (CDIAC) monthly $1^\circ \times 1^\circ$ resolution dataset (Andres et al., 1996, 2011). Each of these component flux datasets was prepared specifically for this 2009–2010 analysis period.

ACPD
12, 29235–29288, 2012

2.1 Model of the carbon cycling in the terrestrial biosphere

VISIT is a prognostic biosphere model (Ito, 2010; M. Saito et al., 2011) that simulates carbon exchanges between the atmosphere and biosphere and among the carbon pools within the terrestrial ecosystems at daily time step. The carbon pools in the model consist of five compartments; foliage, stem and branch, root, litter, and soil. Modeling of plant CO_2 assimilation in VISIT is based on model of light extinction in the canopy, following the formulation of Monsi and Saeki (1953). Maximum photosynthetic uptake rate is influenced by temperature, atmospheric CO_2 concentration, and soil moisture. Autotrophic respiration is formulated as a sum of growth respiration and maintenance respiration. Growth respiration is simulated as the cost to produce new biomass, while maintenance respiration is represented as a function of ground surface temperature. Heterotrophic respiration is formed by the sum of respiration from two layers, litter and humus, which is regulated by soil temperature and soil moisture at each depth. Litter fall from foliage, stems and branches, and roots is calculated by a simple parameterization on the basis of the carbon mass of each component. NEE, which is one of the a priori variables required to drive atmospheric transport model is given as the difference between ecosystem respiration and gross primary productivity. Here, ecosystem respiration is the sum of autotrophic respiration and heterotrophic respiration. A positive value of NEE indicates CO_2 release to the atmosphere from the terrestrial biosphere, whereas a negative value indicates CO_2 uptake from the atmosphere. VISIT is driven by the reanalysis/assimilation climate datasets provided by the Japan meteorological Agency (JMA): the Japan 25-yr reanalysis (JRA-25)/JMA Climate Data Assimilation System (JCDAS) (Onogi et al., 2007) for the period 1979–present. The meteorological data that drives VISIT include downward shortwave radiation at the surface, total cloudiness, 2-m air temperature, ground surface temperature, soil temperature at depths of 10 cm and 200 cm, specific humidity, precipitation, and wind velocity. The JRA-25/JCDAS data are provided at a T106 spatial resolution at 6-h temporal resolution. All of the JRA-25/JCDAS data were converted to daily mean values at a $0.5^\circ \times 0.5^\circ$

ACPD
12, 29235–29288, 2012

grid resolution using an interpolation, which are used as forcing data for VISIT. Biases in JRA-25/JCDAS precipitation data were corrected following the method of Saito, M., et al. (2011). The model was initially run for a spin-up of approximately 2000 yr to reach equilibrium in the carbon pools, by repeating JRA-25/JCDAS forcing with varying atmospheric CO_2. Then the daily physiological processes were simulated were simulated for the period starting in 1979. Global vegetation was classified into 16 plant functional types at a $0.5^{\circ} \times 0.5^{\circ}$ grid resolution using the Moderate Resolution Imaging Spectroradiometer (MODIS) land cover product (Friedl et al., 2002). At each model grid, all physiological processes involve the effect of vegetation fractional coverage up to the fourth dominant biome. We used an optimized VISIT model to provide daily NEE variability. The optimization method and results are described in detail by M. Saito et al., 2013) and are presented only briefly here. Physiological parameters of the model were optimized to fit the observational data by using a Bayesian inversion approach. The observation data for seasonal variability in atmospheric CO_2 concentrations, annual mean aboveground biomass (AGB) and net primary productivity (NPP) were assimilated into VISIT by optimizing physiological parameters in the model for each vegetation type separately. The observation data of atmospheric CO_2, AGB, and NPP were derived from GLOBALVIEW-CO_2 (2010), International Institute for Applied Systems Analysis (IIASA) global biomass map (Kindermann et al., 2008), and Global Primary Production Data Initiative (GPPDI) (Scurlock et al., 1999; Olson et al., 2001), respectively. An atmospheric tracer transport model (Maksyutov et al., 2008) was used in the computation of atmospheric CO_2 variability. Both VISIT and the atmospheric transport model were run on $2.5^{\circ} \times 2.5^{\circ}$ grid resolution. A good match between observations and model simulated seasonal CO_2 cycle while using VISIT fluxes was demonstrated in a forward transport and inverse modeling study by Saeki et al. (2012). Atmospheric transport model simulated atmospheric CO_2 time-series at Mauna-Loa are shown on Fig. 1 in comparison with Globalview-CO2 (2011) along with the biomass maps by VISIT and IIASA.

ACPD
12, 29235–29288, 2012

2.2 Variational assimilation system for simulating the global pCO_2 maps and surface ocean-atmosphere fluxes of carbon

The magnitude of the annual atmospheric CO_2 flux into the oceans is estimated to be 1.5 to 2 PgC yr^{-1} (Gurney et al., 2004; Gruber et al., 2009). Therefore, considerable efforts have been given to the preparation the oceanic fluxes to be used for the GOSAT Level 4 (GOSAT-L4) inversions.

The air-sea CO_2 flux component for this analysis has been taken from an optimal estimate of oceanic CO_2 fluxes derived from the original work of Valsala and Maksyutov (2010). This data set was produced by simulating a dissolved inorganic carbon (DIC) with a simple ocean biogeochemical model and constraining the DIC to observations through a variational assimilation method. The data is available from 1996 to near real-time. The essential components of oceanic CO_2 fluxes utilized as the GOSAT inverse modeling prior are given below.

In the work of Valsala and Maksyutov (2010), a simple offline ocean tracer transport model (OTTM) described by Valsala et al. (2008) is coupled with a simple one-component ecosystem model based on phosphate cycling (McKinley et al., 2004) and abiotic carbon cycle model of OCMIP-II (Ocean Carbon Cycle Intercomparison Project, Orr et al., 1999) and were used to simulate the air-to-sea CO_2 fluxes. The model surface ocean DIC is then constrained with the corresponding observational values that are derived from the observed partial pressure of surface ocean CO_2 (pCO_2) obtained via numerous ship-underway sampling summarised in Takahashi et al. (2007) database. The assimilation consists of a variational method which minimize the model to observation differences in the surface ocean DIC (or pCO_2), using an assimilation method derived from Ikeda and Sasai (2000). The transport model was run with the offline currents provided by GODAS re-analysis data products (Behringer and Xue, 2004). The offline data fed into the system are the ocean current velocities, temperature, salinity and other physical parameters that are derived from the re-analysis data at a five-day time interval. The use of offline re-analysis input fields for running the

ACPD
12, 29235–29288, 2012

transport model enabled us to simulate the air-sea CO_2 flux in a near real-time. The simulated ocean DIC is then corrected via observational data of surface ocean pCO_2 using a two-way constraining process in the assimilation. The model surface ocean pCO_2 are constrained strongly whenever the ship-track underway sampling is available. In addition to this rather "strong" constraint, the climatological maps of monthly mean pCO_2 derived from Takahashi et al. (2009) were also used to constrain the surface ocean pCO_2 as a "weak" constraint. This two-way correction applied to model surface ocean pCO_2 (i.e. effectively to the DIC) reduces the model biases as well as DIC errors. Sixty percent of the annual mean model biases were eliminated in the assimilation, and 40–60 % of the cumulative seasonal errors are also reduced at regional scales (see also Valsala and Maksyutov, 2010).

This operational system of optimal estimates of the air-sea CO_2 flux provides interannually varying oceanic prior fluxes for the inverse flux estimate. Valsala and Maksyutov (2010) used the offline data from the Geophysical Fluid Dynamics Laboratory (GFDL) re-analysis products to drive the transport model. However, because of the fast updates on a near real-time available from the GODAS re-analysis data set we chose to use this data set for our operational estimates of air-sea CO_2 fluxes. Two main advantages of employing the OTTM-derived optimal air-sea CO_2 fluxes as the inversion priors for GOSAT can be summarised as (1) OTTM derived fluxes are monthly varying and available in near real-time, and (2) the air-sea CO_2 fluxes thus have signatures of interannual variability, as compared to the monthly climatological maps of air-sea CO_2 fluxes based on Takahashi et al. (2009), which are often employed in inversion setups (Gurney et al., 2004).

Figure 2 shows the global average of air-to-sea CO_2 fluxes from June 2009 to May 2010, global integrated CO_2 sink and data uncertainties for individual months, used in the inversion. An annual mean of 2.019 $PgC\,yr^{-1}$ of CO_2 sink is resolved in the optimized flux for the period of inversion.

ACPD
12, 29235–29288, 2012

2.3 Emissions dataset for fossil fuel CO_2 emissions

Similar to many other inversion studies (e.g. Gurney et al., 2002), fossil fuel CO_2 emissions (emissions due to combustion of fossil fuels and cement manufacturing) in our inverse estimation are not solved, but rather proscribed. It is thus fossil fuel CO_2 emissions need to be accurately given for better flux estimation (Gurney et al., 2005). To proscribe fossil fuel CO_2 emissions, we used an updated version of the ODIAC dataset (Open-source Data Inventory for Anthropogenic CO_2, Oda and Maksyutov, 2011) prepared at 1×1 degree resolution on monthly basis. Monthly estimates for national total emissions are available from US Department of Energy, Carbon Dioxide Information and Analysis Center (CDIAC) (Boden et al., 2011, http://cdiac.ornl.gov/trends/emis/overview_2008.html, last access: 2 August 2012). These emissions estimates are projected up to year 2010 using BP statistical data (http://www.bp.com/sectionbodycopy.do?categoryId=7500\&contentId=7068481, last access: 2 August 2012) and CDIAC's preliminary estimate (http://cdiac.ornl.gov/trends/emis/prelim_2009_2010_estimates.html, last access: 2 August 2012). The emissions made by CDIAC comprise several fuel and emission categories (solid, liquid and gas fuel, cement production, gas flaring, and international bunkers). Emissions from solid, liquid and gas and cement production were then spatially distributed using power plants profiles (geographical location and emissions) given by CARMA database (CARbon Monitoring and Action, www.carma.org, last access: 6 August 2012) and satellite-observed nightlight data collected by US Air force Defense Meteorological Satellite Project (DMSP) satellites (Elvidge et al., 1999). Nightlight data were processed by National Oceanic and Atmosphere Administration (NOAA) National Geophysical Data Center (NGDC) (Ziskin et al., 2010). This distribution method, compared to previous studies such as Andres et al. (1996), allows us to map emissions over land at a high spatial resolution (up to 1 km) (Oda and Maksyutov, 2011). At spatial resolutions of global transport simulation, the resulting spatial distribution agrees well with that of North American emissions data product Vulcan (Gurney et al., 2009; Oda and Maksyutov,

ACPD
12, 29235–29288, 2012

2011). For other emission categories, emissions from gas flaring are distributed using nightlights dataset specifically processed for gas flaring by NOAA/NGDC (Elvidge et al., 2009, data available from http://www.ngdc.noaa.gov/dmsp/interest/gas_flares.html, last access: 6 August 2012). International bunker emissions are distributed using EDGAR data (http://edgar.jrc.ec.europa.eu/index.php, last access: 2 August 2012) for marine bunkers, and AERO2k inventory (http://www.cate.mmu.ac.uk/aero2k.asp, last access: 2 August 2012) for aviation. In addition to spatial distribution, seasonality in land emissions (solid, liquid, gas and cement) was adopted from CDIAC's monthly 1 × 1 degree emissions dataset (Andres et al., 2011, data available from http://cdiac.ornl.gov/epubs/fossil_fuel_CO2_emissions_gridded_monthly_v2011.html, last access: 2 August 2012). Similarly, AERO2k inventory was used for emissions from aviation. Gas flaring and marine bunker emissions do not have seasonality in ODIAC dataset. Further details are presented in Oda et al. (2012). A global picture of fossil fuel CO_2 emissions is shown in Fig. 3. The figure was drawn using emission data reduced to 5 km × 5 km (2.5 arc min) resolution. Similarly to the emission map by (Oda and Maksyutov, 2011) intensive emissions are found in Northern Hemisphere especially over industrialized countries and regions.

2.4 Emissions of CO_2 by biomass burning and forest fires

Large contribution of the fire processes to the interannual variability of the global carbon cycle is known from high correlation between inversion-reconstructed flux anomalies and satellite based fire estimates (Patra et al., 2005a). Satellite based estimates of the carbon emission due to forest fire and biomass burning are provided by Global Fire Emissions Database (GFED 3.1) as described in (van der Werf et al., 2010; Giglio et al., 2010).

GFED 3.1 used a combination of active fire observations from multiple satellites, 500-m MODIS burned area maps, local regression, and regional regression trees to produce a hybrid, global, monthly burned area data set from July 1996 to December 2010. Annual totals derived from these data show good agreement with independent

ACPD
12, 29235–29288, 2012

annual estimates available for Canada and the United States (Giglio et al., 2010), and Russia (Shvidenko et al., 2011). The global annual burned area for the period 1997–2008 varied between 330 and 431 Mha, with a maximum occurring in 1998 and the minimum in 2008. The most extensive burning consistently occurred in Africa, with an average of 250 Mha burned on the continent each year. This represents about 70 % of the total area burned worldwide annually. The lowest interannual variability the extent of burned areas occurred in the African savannas. Regions of high interannual variability included Australia, the United States, and the boreal forests of both Asia and North America. Burned area maps were produced from the 500-m MODIS atmospherically-corrected Level 2G surface reflectance product (Vermote et al., 2002), the MODIS Level 3 daily active fire products (Justice et al., 2002) and the MODIS Level 3 96-day land cover product (Friedl et al., 2002), by finally applying the Giglio et al. (2009) burned area mapping algorithm. Algorithm validation for 500-m burned area maps is completed for Southern Africa, Siberia, and the Western United States through comparison with Landsat imagery (Giglio et al., 2009). For active fire counts a MODIS monthly Climate Modeling Grid (CMG) fire product at 0.5 deg spatial resolution was used. Detection of fire and burnt area, as well as fraction of the biomass and biomass debris is accompanied by relatively large uncertainties (Giglio et al., 2010) and contribute to the overall uncertainty of the inverse model estimates.

2.5 Atmospheric tracer transport model

We used the National Institute for Environmental Studies global atmospheric tracer Transport Model (NIES TM) to run forward simulations of atmospheric CO_2 for the inverse modeling of surface CO_2 fluxes. The NIES TM is an off-line model driven by reanalysis data, which combines JRA-25 for the period 1979–2004 and a real-time operational analysis by the JMA Climate Data Assimilation System (JCDAS) for the period 2005–present (Onogi et al., 2007). The JRA-25/JCDAS data used in our model is provided on T106 Gaussian horizontal grid (320×160 grid points) with 40 hybrid $\sigma - p$ levels and the 6-h time step. In the version used in this study (version NIES-08.1i), a

ACPD
12, 29235–29288, 2012

flexible hybrid sigma-isentropic ($\sigma - \theta$) vertical coordinate system was implemented, which combines terrain following vertical coordinate in the troposphere and isentropic vertical coordinate in the stratosphere above the level of 350 K to ensure that isentropic surfaces do not intersect the Earth's surface (Belikov et al., 2012a).

A scheme based on radiative heating and cooling was implemented to calculate vertical transport in the stratosphere, because such a scheme produces a better representation of the meridional circulation for long-term simulations, as compared with use of vertical winds from reanalysis (Weaver et al., 1993). Air-ascending rates controlled by climatological heating rate derived from JRA-25/JCDAS reanalysis data were adjusted to fit to the observed mean age of the air in the stratosphere. The model employs a reduced latitude-longitude grid scheme in which the grid size is doubled approaching the poles. This approach overcomes the Courant condition limitation on a model time step in the polar regions, caused by small grid size associated with meridional convergence, maintains a reasonably high integration time-step and ensures adequate model performance (Belikov et al., 2011). The model uses a flux-form advection algorithm with a second-order van Leer scheme. To obtain mass conservation in the numerical scheme, the horizontal mass fluxes derived from the meteorological dataset are balanced with the surface pressure tendency using the method developed by Heimann and Keeling (1989). As in previous model versions (Maksyutov et al., 2008; Belikov et al., 2011) the parameterization of the turbulent diffusivity follows the approach used by Hack et al. (1993). Under the assumption that the planetary boundary layer (PBL) is well mixed the turbulent diffusivity is set to a constant value of $40\,m^2\,s^{-1}$ in the PBL. The free-tropospheric diffusivity is estimated as a function of the Richardson number. To separate the transport processes in the PBL and above it we used 3-hourly PBL height data obtained from the European Centre for Medium-Range Weather Forecasts (ECMWF) Interim Reanalysis dataset (Dee et al., 2011).

We implemented the Kuo-type penetrative cloud convection scheme proposed by Tiedtke (1989), with entrainment and detrainment processes on convective updrafts and downdrafts to simulate deep convection (Belikov et al., 2012b). Calculation of

ACPD
12, 29235–29288, 2012

cumulus mass-flux is based on the method developed by Austin and Houze (1973), in which the amount of air lifting in an updraft core of a cumulus cell is related the amount of precipitation the cumulus cell produces. The mass of air transported upward within the cells was computed from the conservation of moisture, using the convective precipitation rate from the JRA-25/JCDAS dataset.

The model was evaluated against GLOBALVIEW-CO2, GLOBALVIEW-CH4, World Data Centre for Greenhouse Gases (WDCGG), balloon-borne and aircraft observation data (Belikov et al., 2011, 2012a), as well as through the Comprehensive Observation Network for Trace gases by AIrLiner (CONTRAIL) (Niwa et al., 2011) and TransCom-CH_4 transport model intercomparison (TMI) studies (Patra et al., 2011; Belikov et al., 2012b). Implementation of hybrid sigma-isentropic vertical coordinates with a radiative balance scheme of vertical transport allows simulation of vertical profiles and vertical propagation of seasonal variations of tracers in the free troposphere and in the lower stratosphere which appears to be in good agreement with aircraft and balloon-borne observations. In general NIES TM performance is consistent with the TransCom-CH_4 and CONTRAIL intercomparison participating models (Niwa et al., 2011; Patra et al., 2011). Comparisons with balloon-borne observations over Sanriku, Japan in 2000–2007 revealed that the tracer transport simulations in the upper troposphere and lower stratosphere are performed with accuracies of ∼5 % for CH_4 and SF_6, and ∼1 % for CO_2 compared with the observed volume-mixing ratios (Belikov et al., 2012a).

The model is able to reproduce the seasonal variations in CO_2 and CH_4 surface concentrations. More accurate results were obtained for CH_4 at regions located some distance away from multiple emission sources. For other sites, where high emissions and local meteorology play a major role, it proved difficult to reproduce the CH_4 surface concentrations, especially in winter, which indicates excessive near-surface vertical mixing under stable conditions.

Modelled dry-air column-averaged CO_2 and CH_4 values (X_{CO_2} and X_{CH_4}) were also evaluated against daily ground-based high-resolution FTS observations measured at 12 TCCON sites for the period from January 2009 to January 2011. Modeled data

ACPD
12, 29235–29288, 2012

convolved with scene-dependent averaging kernels were able to reproduce the seasonal and inter-annual variability of X_{CO_2} and X_{CH_4} with correlation coefficients of 0.8–0.9 and 0.4–0.8, and biases ± 0.2 % and ± 0.5 % (without Sodankyla's data), respectively (Belikov et al., 2012a).

3 Inverse modeling scheme

Atmospheric inversion is a technique that has been commonly employed for inferring surface source strengths of CO_2 from measurements of CO_2 concentrations. The theoretical basis for the technique is Bayes' theorem (see e.g. Tarantola, 2005), with which the "optimal" or a posteriori state of a set of parameters is deduced from a priori knowledge about those parameters and measured data values. For the case of estimating surface fluxes of chemically inert gas species, such as CO_2, the relationship between the measured data values and their theoretical predictions based on physical process modeling is linear. The relationship can be expressed in matrix form as

$$\boldsymbol{d}_{\text{obs}} = \mathbf{G}\boldsymbol{m} + \boldsymbol{v} \quad (1)$$

where $\boldsymbol{d}_{\text{obs}}$ is the concentration vector recorded at measurement locations, $\boldsymbol{m}$ denotes modeled source strengths in pre-defined spatial boundaries, and $\mathbf{G}$ is a matrix that maps the source strength field onto that of concentrations. The elements of matrix $\mathbf{G}$ are given as changes in concentrations at each of measurement sites with respect to unit pulse emissions from each of the pre-defined spatial boundaries. These elements are obtained by running forward a set of unit pulse emissions with an atmospheric tracer transport model (e.g. Rayner et al., 1999). Vector $\boldsymbol{v}$ is the misfit between the observations and the model-predictions, which is comprised of measurement uncertainty and error in the simulation of atmospheric transport. The aim here is to find $\boldsymbol{m}$ that best describes $\boldsymbol{d}_{\text{obs}}$. In the context of Bayesian inference, where Gaussian probabilities are assumed for measurements and a priori parameters, the measure of the fit between

ACPD
12, 29235–29288, 2012

modeled source strengths $\boldsymbol{m}$ and measurements is expressed as a cost function $L(\boldsymbol{m})$ (also see Tarantola, 2005):

$$L(\boldsymbol{m}) = \frac{1}{2}(\mathbf{G}m - \boldsymbol{d}_{\text{obs}})\mathbf{C}_{\text{D}}^{-1}(\mathbf{G}m - \boldsymbol{d}_{\text{obs}}) + \frac{1}{2}(\boldsymbol{m} - \boldsymbol{m}_{\text{prior}})\mathbf{C}_{\text{M}}^{-1}(\boldsymbol{m} - \boldsymbol{m}_{\text{prior}}), \quad (2)$$

where $\boldsymbol{m}_{\text{prior}}$ denotes the vector of the a priori source strengths, and $\mathbf{C}_{\text{D}}$ and $\mathbf{C}_{\text{M}}$ are the error covariance matrices of the measurements and the a priori source strengths, respectively. The optimal state of the modeled source strengths, $\boldsymbol{m}'$, exists at the minimum of this measure. Taking the derivative of L with respect to $\boldsymbol{m}'$ and setting it to zero yields

$$\boldsymbol{m}' = \boldsymbol{m}_{\text{prior}} + (\mathbf{G}^{\text{T}}\mathbf{C}_{\text{D}}^{-1}\mathbf{G} + \mathbf{C}_{\text{M}}^{-1})^{-1}\mathbf{G}^{\text{T}}\mathbf{C}_{\text{D}}^{-1}(d_{\text{obs}} - \mathbf{G}\boldsymbol{m}_{\text{prior}}). \quad (3)$$

Further, differentiating L with respect to $\boldsymbol{m}$ for the second time gives the a posteriori error covariance, $\mathbf{C}'_{\text{M}}$,

$$\mathbf{C}'_{\text{M}} = (\mathbf{G}^{\text{T}}\mathbf{C}_{\text{D}}^{-1}\mathbf{G} + \mathbf{C}_{\text{M}}^{-1})^{-1}, \quad (4)$$

which is a measure of the convexity of the function L.

The values assigned to the elements of vector $\boldsymbol{d}_{\text{obs}}$ in the present study were monthly-mean, surface-based GV observations and bias-corrected GOSAT X_{CO_2} retrievals gridded to $5^\circ \times 5^\circ$ cells and averaged on a monthly basis. Cells with three or more X_{CO_2} retrievals per month were used. Prior to monthly averaging, large GOSAT X_{CO_2} outliers were removed via comparisons with climatological X_{CO_2} values, derived from an ensemble of forward simulation results by six different transport models that was nudged to surface-based observations (R. Saito et al., 2011). The observation errors for the monthly mean X_{CO_2} retrievals, specified in the diagonal elements of matrix $\mathbf{C}_{\text{D}}$, were determined as the standard deviations of GOSAT X_{CO_2} retrievals found in each of the $5^\circ \times 5^\circ$ grid cells in a month. We took account of errors associated with the retrieval of X_{CO_2} values and the forward atmospheric transport simulation by setting the minimum of the observation error for the GOSAT X_{CO_2} retrievals at 3 ppm (a conservative estimate). The GV sites were selected by comparing GV observations against

ACPD
12, 29235–29288, 2012

concentrations predicted by the NIES-TM over the analysis period. We picked the sites whose RMS model-observation misfits were less than 2 ppm. As an observation error estimate, the GV residual standard deviation (stored in the GV dataset) was assigned to each of the selected sites. We gave less weight at GV sites whose observational record completeness was less than 70 % by tripling their data errors. The minimum error for the GV observations was set to 0.3 ppm. Altogether, 220 GV sites were selected for this estimation.

The diagonal elements of the matrix $\mathbf{C}_M$ were prescribed as follows. The uncertainty of the terrestrial a priori flux was set at twice the standard deviation of the VISIT model monthly NEE ($1^\circ \times 1^\circ$ resolution) values for the past 30 yr. The uncertainty of the oceanic a priori flux was determined as the standard deviation of the OTTM-assimilated oceanic flux ($1^\circ \times 1^\circ$ resolution) for the period 2001–2009, and the climatological mean data of Takahashi et al. (2009).

The size of vector $\boldsymbol{m}$ in the present study was set to the number of source regions (64 regions) times the number of analysis months (14 months). The 64 source regions consist of 42 subcontinental-scale terrestrial regions and 22 ocean basins, following Patra et al. (2005b). The boundaries of these source regions are shown in Fig. 4. The dimension of matrix $\mathbf{G}$ is then determined as the size of vector $\boldsymbol{m}$ multiplied by that of vector $\boldsymbol{d}_{\mathrm{obs}}$. For implementing matrix operations involved in Eq. (3) efficiently, we employed a variant of the fixed-lag Kalman Smoother scheme (FLKS) formulated by Bruhwiler et al. (2005). The basis for this scheme is the fact that in atmospheric tracer transport simulations, the signals of unit pulse emissions detected at measurement sites decay rapidly within the first few months and are blended into the background state thereafter. The idea is to obtain a posteriori fluxes via estimating $\boldsymbol{m}'$ incrementally with a subset of $\mathbf{G}$ and $\boldsymbol{d}_{\mathrm{obs}}$ in a specified time-window. Using the FLKS setup with the same 64 source region boundaries, Koyama et al. (2009) evaluated the influence that the difference in the length of the time window has on a posteriori monthly flux estimates. Comparing results obtained using window lengths of 1 to 6 months, they concluded that a posteriori fluxes and their uncertainties estimated with three-month

ACPD
12, 29235–29288, 2012

or longer windows converged quite strongly; Bruhwiler et al. (2005) arrived at a similar conclusion. Based on these findings, we chose to use a three-month duration of monthly observations and atmospheric transport simulations in each time window.

In implementing the scheme, only random errors associated with the prior fluxes and observations, as specified in matrices $\mathbf{C}_D$ and $\mathbf{C}_M$, are accounted for. Thus, biases in the observations need to be removed prior to the optimization. We placed two additional columns in matrix **G** that correspond to global CO_2 offsets of (1) the initial model concentrations with respect to the GV observations, and (2) the GOSAT X_{CO_2} retrievals with respect to the GV observations. These two independent values, determined in an initial optimization run, were used in the subsequent run to remove the global offsets.

3.1 GOSAT X_{CO_2} retrievals

The main observational instrument aboard GOSAT is the Earthward-looking TANSO-FTS that measures surface-reflected sunlight and emitted thermal infrared radiation at wavelengths in the range 0.76–14.3 µm. The design and functions of the instrument are described in detail by Kuze et al. (2009). Sampled spectra recorded in the 0.76-µm oxygen absorption band and the 1.61-µm CO_2 absorption band were used in an earlier version of the NIES Level 2 operational retrieval algorithm (version 01; described by Yoshida et al., 2011) to retrieve X_{CO_2} global distributions. The retrieved X_{CO_2} values exhibited promising characteristics, including distinct north–south gradients and seasonal variability. However, the X_{CO_2} values were found to contain a significant negative bias of 8.85 ± 4.75 ppm (Morino et al., 2011) as compared with reference data collected at observational sites of the Total Carbon Column Observing Network (TCCON) (Wunch et al., 2011), where sun-viewing high-resolution FTSs are installed. Later, Uchino et al. (2012), using their lidar observations of aerosol particles, showed that assumptions made in version 01 of the retrieval algorithm on the vertical distributions of thin cirrus and aerosols are oversimplified, thereby contributing to the large bias. They proved that the issue could be mitigated significantly by the use of aerosol/cirrus optical properties retrieved simultaneously with spectra in the 2.06 µm

ACPD
12, 29235–29288, 2012

band. Further, through investigating GOSAT spectra sampled over 2.5 yr, Yoshida et al. (2012) discovered a time-dependent degradation of TANSO FTS's radiometric accuracy, which they successfully modeled for use in the retrieval algorithm implementation. These new findings, along with other improvements, were incorporated into the NIES Level 2 operational retrieval algorithm. The updated Level 2 X_{CO_2} retrievals (version 02.00), processed from an improved GOSAT spectral dataset (Level 1B data, version 141.141, covering 14 months from June 2009 to July 2010) were shown to have a much smaller bias of -1.20 ± 1.97 ppm (Yoshida et al., 2013). However, the causes of the remaining bias require further investigation. The results presented hereafter in this paper are based on this version of the data product.

Figure 5 shows the number of GOSAT X_{CO_2} retrievals per each of $5^\circ \times 5^\circ$ cells counted during the months of August 2009, November 2009, February 2010, and May 2010. The distribution of the data number density changes with season owing to the occurrence of clear sky days and local solar zenith angle that determines the northern- and southern-most bounds of the GOSAT measurement. Note here that regions above $\sim 50^\circ$ N latitude (the northern parts of North America and Eurasia) during fall and winter months saw very small numbers of GOSAT retrievals therefore the flux inference for those regions in those months was reliant on the GV observations. Figure 6 displays the ver. 02.00 of the GOSAT X_{CO_2} retrievals in the form of input to the inverse modeling scheme (gridded to $5^\circ \times 5^\circ$ cells and averaged on a monthly time scale). Only the cells with three or more retrievals per month are shown here. Prior to monthly averaging, we corrected the bias in the GOSAT X_{CO_2} retrievals by raising each X_{CO_2} value by 1.20 ppm, assuming that the bias is uniform throughout the globe and the observation period. Evaluating the reasonableness of this assumption is a subject of ongoing studies. The monthly mean GV values are also shown in the figure in circles.

3.2 Treatment of GOSAT averaging kernel

To account for the vertical sensitivity of the GOSAT measurement in the inverse modeling, we applied the averaging kernel, derived in the retrieval of X_{CO_2}, to each of the

ACPD
12, 29235–29288, 2012

vertical concentration profiles simulated with NIES-TM. As was described by Connor et al. (2008), a model-simulated X_{CO_2} concentration $X^{m}_{CO_2}$, which reflects the measurement vertical sensitivity, is given as:

$$X^{m}_{CO_2} = X^{a}_{CO_2} + \sum_i (\boldsymbol{h}^{T}\mathbf{A})_i (x_m - \boldsymbol{x}_a)_i, \quad (5)$$

where $X^{a}_{CO_2}$ denotes a priori X_{CO_2} value defined in the X_{CO_2} retrieval; **A** is a matrix containing the CO_2 elements of the averaging kernel; $\boldsymbol{x}_m$ and $\boldsymbol{x}_a$ denote the elements of the modeled and the a priori vertical CO_2 profile, respectively. $\boldsymbol{h}$ is the pressure weighting function, a vector containing the dry air partial column abundance of each retrieval layer normalized to the total dry air column abundance. The calculation of the pressure weighting function is described in Appendix B of a report by Yoshida et al. (2009).

4 Results and discussion

Using the 14-month-long GOSAT Level 2 X_{CO_2} retrievals (version 02.00) and the GV observations in the 3-month-window FLKS scheme, we inferred monthly fluxes for the 64 subcontinental regions for 12 months between June 2009 and May 2010. The forward concentration simulation was initialized with a GECM-derived 2-D global concentration field, and the pre-run was performed for 3 months before the start of the inversion period. A total of 9106 observations were available for estimating 768 monthly fluxes (64 regions × 14 months), of which 6125 were gridded monthly-mean GOSAT X_{CO_2} retrievals and 2981 were monthly-mean GV observations.

The reduction in the a priori flux uncertainty corresponds to the degree to which observations used in the inference contributed to constraining the surface fluxes. The reduction is often expressed by contrasting the diagonal parts of the a posteriori error covariance matrix, $\mathbf{C}'_M$, to that of the a priori one, $\mathbf{C}_M$. Here, we rather chose to consider the uncertainty reduction attained by the addition of the GOSAT X_{CO_2} retrievals to the

ACPD
12, 29235–29288, 2012

GV observations. Following Rayner and O'Brian (2001) and Takagi et al. (2011), we the uncertainty reduction (UR) as:

$$\mathrm{UR} = \left(1 - \frac{\sigma_{\mathrm{GV+GOSAT}}}{\sigma_{\mathrm{GV}}}\right) \times 100, \quad (6)$$

where the units of UR are in %, and σ_{GV} and $\sigma_{\mathrm{GV+GOSAT}}$ denote the uncertainties in the monthly flux estimated from the GV observations only and those from both the GV observations and the GOSAT retrievals, respectively. For this evaluation, we implemented the inversion scheme using only the GV observations to obtain flux estimates and the value of σ_{GV}. Figure 7 presents the UR values for August 2009, November 2009, February 2010, and May 2010. As indicated in Eq. (4), the value of UR is affected by three factors: (1) the uncertainty in the observations and a priori fluxes, given by $\mathbf{C}_{\mathrm{D}}$ and $\mathbf{C}_{\mathrm{M}}$, respectively; (2) the sensitivity of observations to surface fluxes (determined by atmospheric transport and stored in $\mathbf{G}$); and (3) the size of $\mathbf{C}_{\mathrm{D}}$, which reflects the number of observations available for constraining the fluxes. Note that in the current inversion setup the uncertainties specified for GV observations and that for GOSAT retrievals can differ by as much as one order of magnitude (e.g. the minimum uncertainty set for GV observations and GOSAT retrievals is 0.3 and 3.0 ppm, respectively). This implies that the GV observations have much greater weight in constraining regional fluxes. Also we consider that there is approximately one-order-of-magnitude difference between the uncertainties prescribed to land fluxes and to ocean fluxes. These differences contribute to creating strong region-to-region or land-to-ocean contrasts in UR values, as observed in Fig. 7. Regions that are far from ground-based observation networks but are covered by GOSAT retrievals (e.g. Regions 29 and 17; see Fig. 4 for identifying the regions) show higher UR values, with a maximum UR of 61 % for Region 29 in October 2009 (not shown in the figure). However, the UR values for the North American and Australian regions (regions 5–8 and 35–38) barely exceed ~ 15 %, despite the fact that GOSAT retrievals were constantly available within and around these regions throughout the 1-yr analysis period (see Fig. 6). This represents a case in which the

ACPD
12, 29235–29288, 2012

constraint provided by the GV observations prevails over that provided by the GOSAT X_{CO_2} retrievals. Thus, higher URs in the figure highlight regions whose a posteriori fluxes were constrained by the GOSAT retrievals more strictly than those in other regions (Middle East, Asia, Africa, and South America). In light of the GOSAT mission objectives, Fig. 7 indicates what the satellite was designed to perform in complementing the ground-based observations. However, care must be taken in evaluating the flux values, as these remote regions coincide with locations where the validation of GOSAT retrievals is not currently possible and the retrieval of X_{CO_2} values itself is challenged by higher local surface albedo and/or contamination by aerosols.

Figure 8 shows the monthly a posteriori fluxes described above. The quantity presented here is the sum of a priori fluxes (terrestrial biosphere exchange or ocean exchange + anthropogenic emissions + forest fire emissions) and the correction to the a priori flux determined via the optimization. The net influence of the addition of the GOSAT X_{CO_2} retrievals to the GV observations on the flux estimation is made visible by taking the difference between the flux correction obtained with GV observations only and that with both the GV observations and the GOSAT retrievals (see Fig. 9). As indicated by the distribution of UR rates shown in Fig. 7, the major changes in the correction fluxes occurred in the data-poor regions of surface observation networks. Among the changes, those associated with very low URs ($<\sim 15\,\%$; e.g. tropical America, central Africa, and southern Asia in summer and spring) need to be isolated as they are most likely the result of flux balancing or compensation that took place through the optimization of neighboring regional fluxes. The remaining changes, which are associated with higher URs (e.g. northern Eurasia during summer, the Middle East, southern Africa, and central Asia) and therefore more strongly linked to the GOSAT X_{CO_2} retrievals, are explored further here. The site-by-site GOSAT data validation activities showed that the X_{CO_2} retrievals now agree reasonably well with the TCCON reference dataset, with a global mean bias of -1.20 ± 1.97 ppm. Evaluating the validity of spatiotemporal changes in the global distribution of GOSAT-based X_{CO_2} concentrations

ACPD
12, 29235–29288, 2012

will, however, continue to present challenges, perhaps until the cross-validation of similar space-based CO_2 measurements is possible.

Here, we describe attempts to perform such an evaluation using a model-simulated 3-D CO_2 field as an independent reference. We constructed this reference field by running forward with the NIES-TM a posteriori fluxes estimated from the GV observations only (mentioned earlier in this section). The quality of this GV-based global CO_2 field was examined with the TCCON references. Figure 10 shows the monthly time series data collected at five TCCON sites (Ny Ålesund, Norway; Bialystok, Poland; Park Falls, USA; Tsukuba, Japan; and Wollongong, Australia; described in: Wunch et al., 2011; Washenfelder et al., 2006; Messerschmidt et al., 2010, 2012; Deutscher et al., 2010; Ohyama et al., 2009, respectively) and the corresponding forward simulation results. As summarized in Table 1, the misfits between TCCON and GV-based model predictions are mostly within the range of observational uncertainties. Figure 11 compares the distribution of the $5^\circ \times 5^\circ$ GOSAT X_{CO_2} values with the reference field (monthly-mean GOSAT X_{CO_2} minus the corresponding reference X_{CO_2} concentrations). Positive or negative deviations from the GV-based CO_2 reference greater than 2 ppm, which is larger than the range of TCCON uncertainty and model-observation misfits, are found in lower South America (August and May), equatorial Africa (November and February), and central Asia (August and May).

When compared with the distributional patterns of values shown in Fig. 7, the locations of enhanced deviations from the reference coincide well with regions of higher UR values, which are indicative of greater involvement of GOSAT X_{CO_2} retrievals in the flux estimation. From the limited view point of this particular GV-based CO_2 concentration reference, we note that the changes in fluxes observed in Fig. 9 are likely induced by the GOSAT X_{CO_2} retrievals. This point is, of course, strictly subject to changes made in the current minimum observational uncertainty settings, which can increase the competition between GV observations and GOSAT retrievals in constraining fluxes, or to improvements made in constructing the modeled CO_2 reference field (e.g. augmenting

ACPD
12, 29235–29288, 2012

the GV observations used in estimating the surface-based fluxes by adding other available surface observations).

To illustrate the effects of adding GOSAT X_{CO_2} retrievals to the GV observations on the seasonality of the estimated fluxes, we plotted in Fig. 12 the time series of fluxes over the one-year analysis period for June 2009 to May 2010 for southern Africa (regions 21-24) and boreal Eurasia (region 25–28). The fluxes of these selected regions are underconstrained by surface observations and the fluxes change with the addition of GOSAT observations. The fluxes for most regions and seasons remained within natural variability bounds, which also served as a priori constrains. Winter fluxes of northern boreal Eurasia appear to be variable and underconstrained as the seasonal variability was not reflected in the a priori flux uncertainties.

The practical value of GOSAT observations to inverse modeling of surface fluxes can be confirmed if the estimated fluxes are more accurate than those in the case without GOSAT observations. Direct validation with independent regional flux estimates, such as those being developed by Canadell et al. (2011), would be an attractive option, but the data for our analysis period are not yet available. A common approach in inverse modeling is to examine statistics of the difference between the prior and posterior fluxes (Tarantola, 2005). In our case we can evaluate the change in the difference between the prior and posterior fluxes that is due to the addition of GOSAT observations. For 12 land regions (numbered 05, 06, 09, 10, 12, 14, 15, 26, 29, 32, 33, 39, see region numbers on Fig. 4), the addition of GOSAT observations moves the estimated fluxes closer to the prior fluxes as compared with using only GV observations, thereby reducing the misfit between prior and posterior fluxes. However, the opposite is seen for other seven regions (16, 17, 18, 22, 25, 27, 42). It is not always clear if the deviations from the prior fluxes are in the right or wrong direction; for example, in regions 25 and 27 (western boreal Eurasia), the addition of GOSAT data increases the summer uptake, while evidence from another study indicates that the use of our prior fluxes results in the simulation of a seasonal cycle with a lower amplitude as compared with surface observations over Siberia (Saeki et al., 2012).

ACPD
12, 29235–29288, 2012

To illustrate the effect of GOSAT observations on the estimated fluxes, Fig. 13 shows the changes of the difference between prior and posterior fluxes caused by adding the GOSAT retrievals. Here we chose only those regions and months for which the UR was larger than 20 % (a total of 80 monthly regional flux values). Change in the fluxes is described as follows:

$$\Delta \boldsymbol{m}^2 = \left(\boldsymbol{m}_{\mathrm{GV}} - \boldsymbol{m}_{\mathrm{prior}}\right)^2 - \left(\boldsymbol{m}_{\mathrm{GV+GOSAT}} - \boldsymbol{m}_{\mathrm{prior}}\right)^2, \quad (7)$$

where $\boldsymbol{m}_{\mathrm{GV}}$ is the flux estimated with GV-only observations and $\boldsymbol{m}_{\mathrm{GV+GOSAT}}$ is the flux estimated with GV observations combined with GOSAT. A positive value of $\Delta \boldsymbol{m}^2$ means the deviation from the prior is reduced (i.e., the estimated flux becomes closer to the prior) and negative $\Delta \boldsymbol{m}^2$ indicates that the addition of GOSAT moves the estimated flux away from the prior value. For small changes in fluxes (~ 1 PgC/year/region) the effect of GOSAT observations is statistically similar for both positive and negative changes. In contrast, a number of large positive $\Delta \boldsymbol{m}^2$ values clearly indicate that the addition of GOSAT observations acts to suppress many large and likely erroneous deviations from prior fluxes in the regions where fluxes are underconstrained when estimations are made with GV observations alone.

As discussed by Gurney et al. (2002, 2004), the problem of underconstrained regions in inversions is not limited to the large estimated flux uncertainties: the estimated fluxes themselves appear more variable in terms of departure from the prior flux, with a large spread arising when different transport models are used with the same observation data. A reduction in the difference between estimated and prior fluxes for underconstrained regions with the introduction of GOSAT observations would confirm two points. First, a reduction in theoretically estimated flux uncertainty corresponds to a reduction in the deviation of the estimated fluxes themselves from prior fluxes. Second, observations by GOSAT on average do not contradict with prior flux estimates; otherwise, the addition of GOSAT observations to the inverse model would increase deviations of the flux estimates from prior, while claiming a reduction in flux uncertainty at the same time.

ACPD
12, 29235–29288, 2012

Estimates of annual global total flux are useful for evaluating the validity of inverse modeling results. The global total flux for a one-year analysis period (June 2009 to May 2010) was estimated to be 4.75 GtC yr^{-1} (land/ocean: −2.09/−2.00 GtC yr^{-1}) for GV-only data, and 5.18 GtC yr^{-1} (land/ocean: −1.19/−2.48 GtC yr^{-1}) for GV combined with GOSAT. Although land-ocean partitioning appears within the range of other model estimates, the difference in global total flux between the two sets of observational data is indicative of some regional and temporal differences between GOSAT observations and the model-simulated X_{CO_2} distribution based on the inversion with GV-only data. Characterizing the temporal and spatial distribution of the CO_2 growth rate for this period (2009–2010) is complicated by high temperatures observed in the Northern Hemisphere during the first half of 2010 (Galarneau et al., 2012), which were followed by a heat wave and a large forest fires in western Russia (Barriopedro et al., 2011; Shvidenko et al., 2011). Further investigations are needed regarding the spatiotemporal variability of the biases in the current X_{CO_2} retrievals.

5 Summary and conclusions

We developed an integrated global carbon cycle modeling system designed specifically for analysis of the GOSAT X_{CO_2} observations and estimating the seasonal and interannual variations of regional CO_2 fluxes. The forward modeling components, the NIES atmospheric transport model, the ODIAC fossil fuel emission inventory, the VISIT terrestrial biosphere exchange model and the oceanic pCO_2 data assimilation system were optimized to match the seasonal, interannual and spatial variability of the atmospheric CO_2 and surface CO_2 fluxes. For better simulating X_{CO_2} concentrations, the stratospheric transport was simulated on an isentropic grid and was tuned to reproduce the stratospheric air age. The fossil fuel emission inventory, based on use of large point source data and night lights observations, improved the spatial distribution of CO_2 emissions that was confirmed to correlate well with detailed bottom up inventory at the horizontal resolutions of 0.5° to 1° . The parameters in the terrestrial biospheric

ACPD
12, 29235–29288, 2012

model VISIT were optimized to simultaneously fit the observed atmospheric CO_2 seasonal cycle, observations of the net primary production and biomass distribution map. Oceanic surface CO_2 fluxes were simulated with oceanic 4-D variational data assimilation system based on reanalyzed ocean currents, using available pCO_2 observations and global oceanic pCO_2 climatology as constraints. A recent version of the global fire emission database (GFED) was used to account for fire emissions.

The inverse modeling approach optimizing monthly mean fluxes for 64 regions (Patra et al., 2005b) was extended to using GOSAT observations. The fixed-lag Kalman Smoother scheme was implemented in the flux estimation. The inverse model takes into account the effects of prior CO_2 profiles on retrieval provided with column averaging kernel data. A globally constant offset between ground-based in-situ observations and GOSAT retrievals is estimated as optimized parameter. The GOSAT X_{CO_2} data screening is implemented using an observation-adjusted 3-D CO_2 concentration climatology. To confirm the consistency between simulated variations of the ground based and total column data, the X_{CO_2} data obtained by inverse model fit to GV observations were compared with TCCON observations and good agreement was found.

The inverse modeling system was then applied to analysis of the CO_2 observations combining the GV ground based and aircraft observations and GOSAT X_{CO_2} data. The inverse model fluxes estimated using both GV and GOSAT data appear to be close to those estimated using GV for regions well constrained by GV observations. On the other hand, the fluxes change considerably when the data by GOSAT are added for regions remote from GV observations, which are accompanied with sizeable estimated flux uncertainty reductions for those regions.

Variability of the estimated monthly fluxes was considerably reduced as compared with former version mainly due to significantly reduced scatter of Level 2 data. For most of the regions and seasons the estimated fluxes fall within a range of natural flux variability estimated with component models. The analysis of the estimated regional flux data and annual mean flux suggests that more improvements in the quantification

ACPD
12, 29235–29288, 2012

and correction of the X_{CO_2} Level 2 data biases are desirable. There is a need for a coordinated effort to check and validate the regional monthly CO_2 flux estimates.

Supplementary material related to this article is available online at: http://www.atmos-chem-phys-discuss.net/12/29235/2012/acpd-12-29235-2012-supplement.pdf.

Acknowledgements. The GOSAT Project is a joint undertaking of three organizations: the Japan Aerospace Exploration Agency, the National Institute for Environmental Studies (NIES), and the Japanese Ministry of the Environment. The work benefited from support and efforts contributed by P. K. Patra, P. Rayner, T. Nakazawa, G. Inoue, Y. Sasano, H. Akimoto, M. Ikeda, Y. Nakatsuka, Y. Koyama, N. Kadygrov, A. Yaremchuk, M. Naja, H.-S. Kim, T. Machida, Y. Nojiri, T. Shirai, S. Oshchepkov, A. Bril and discussions with H. Mukai, L. Feng, F. Chevallier, S. Houweling, P. Peylin and Transcom project members. Authors would like to thank the members of the GOSAT Project for their contribution to this work. M. Harada, K. Matsubara, and colleagues at AdvanceSoft Corp. contributed to the development of data processing systems. The NIES supercomputer system (including NEC SX-8R/128M16) was used for the development and implementation of the inverse modeling system components. Globalvew-CO_2 dataset used in this study is contributed by cooperating scientists and their organizations. The datasets used for this study were provided by the cooperative research project of the JRA-25/JCDAS long-term reanalysis by Japan Meteorological Agency (JMA) and Central Research Institute of Electric Power Industry (CRIEPI). TCCON data made available to us due to efforts by P. Wennberg, J. Notholt, N. Deutcher, D. Griffith, D. Wunch and a number of contributing scientists. Funding for TCCON is provided by NASA's Terrestrial Ecology Program (grant NNX11AG01G), the Orbiting Carbon Observatory Program, the Atmospheric CO_2 Observations from Space (ACOS) Program, and the Department of Energy/Atmospheric Radiation Measurement (DOE/ARM) Program. We acknowledge funding to support Wollongong site from the Australian Research Council, projects LE0668470, DP0879468, DP110103118 and LP0562346. We acknowledge financial support of the Białystok TCCON site from the Senate of Bremen and EU projects IMECC, GEOMON and InGOS as well as maintenance and logistical work provided by AeroMeteo Service (Białystok) and the RAMCES team at LSCE (Gif-sur-Yvette, France) and additional

ACPD
12, 29235–29288, 2012

operational funding from the NIES GOSAT project. RJA was sponsored by U.S. Department of Energy, Office of Science, Biological and Environmental Research (BER) programs and performed at Oak Ridge National Laboratory (ORNL) under U.S. Department of Energy contract DE-AC05-00OR22725.

References

Andres, R. J., Marland, G., Fung, I., and Matthews, E. A.: $1^{\circ} \times 1^{\circ}$ distribution of carbon dioxide emissions from fossil fuel consumption and cement manufacture, 1950–1990, Global Biogeochem. Cy., 10, 419–429, 1996.

Andres, R., Gregg, J. S., Losey, L., Marland, G., and Boden, T.: Monthly, global emissions of carbon dioxide from fossil fuel consumption, Tellus, 63B, 309–327, 2011.

Austin, P. M. and Houze Jr., R. A.: A technique for computing vertical transports by precipitating cumuli, J. Atmos. Sci., 30, 1100–1111, 1973.

Barriopedro, D., Fischer, E. M., Luterbacher, J., Trigo, R. M., and García-Herrera, R.: The hot summer of 2010: Redrawing the temperature record map of Europe, Science, 332, 220–224, 2011.

Behringer, D. W. and Xue, Y.: Evaluation of the global ocean data assimilation system at NCEP, in: The Pacific Ocean. Eighth symposium on integrated observing and assimilation system for atmosphere, ocean, and land surface, AMS 84th annual meeting, Seattle, Washington, DC, 11–15, 2004.

Belikov, D., Maksyutov, S., Miyasaka, T., Saeki, T., Zhuravlev, R., and Kiryushov, B.: Mass-conserving tracer transport modelling on a reduced latitude-longitude grid with NIES-TM, Geosci. Model Dev., 4, 207–222, doi:10.5194/gmd-4-207-2011, 2011.

Belikov, D. A., Maksyutov, S., Sherlock, V., Aoki, S., Deutscher, N. M., Dohe, S., Griffith, D., Kyro, E., Morino, I., Nakazawa, T., Notholt, J., Rettinger, M., Schneider, M., Sussmann, R., Toon, G. C., Wennberg, P. O., and Wunch, D.: Simulations of column-average CO_2 and CH_4 using the NIES TM with a hybrid sigma-isentropic ($\sigma - \theta$) vertical coordinate, Atmos. Chem. Phys. Discuss., 12, 8053–8106, doi:10.5194/acpd-12-8053-2012, 2012a.

Belikov, D. A., Maksyutov, S., Krol, M., Fraser, A., Rigby, M., Bian, H., Agusti-Panareda, A., Bergmann, D., Bousquet, P., Cameron-Smith, P., Chipperfield, M. P., Fortems-Cheiney, A., Gloor, E., Haynes, K., Hess, P., Houweling, S., Kawa, S. R., Law, R. M., Loh, Z., Meng,

ACPD
12, 29235–29288, 2012

L., Palmer, P. I., Patra, P. K., Prinn, R. G., Saito, R., and Wilson, C.: Off-line algorithm for calculation of vertical tracer transport in the troposphere due to deep convection, Atmos. Chem. Phys. Discuss., 12, 20239–20289, doi:10.5194/acpd-12-20239-2012, 2012b.

Boden, T. A., Marland, G., and Andres, R. J.: Global, Regional, and National Fossil-Fuel CO_2 Emissions. Carbon Dioxide Information Analysis Center, Oak Ridge National Laboratory, U.S. Department of Energy, Oak Ridge, Tenn., USA, available at: http://cdiac.ornl.gov/trends/emis/overview_2008.html (last access: November 2012), 2011.

Bousquet, B., Peylin, P., Ciais, P., Le Quéré, C., Friedlingstein, P., and Tans, P. P.: Regional Changes in Carbon Dioxide Fluxes of Land and Oceans Since 1980, Science, 290, 1342–1346, 2000.

Bösch, H., Baker, D., Connor, B., Crisp, D., and Miller, C.: Global Characterization of CO_2 Column Retrievals from Shortwave-Infrared Satellite Observations of the Orbiting Carbon Observatory-2 Mission, Remote Sens., 3, 270–304, 2011.

British Petroleum p.l.c., Statistical Review of World Energy 2011, available at: www.bp.com/statisticalreview (last access: July 2012), 2011.

Bruhwiler, L. M. P., Michalak, A. M., Peters, W., Baker, D. F., and Tans, P.: An improved Kalman Smoother for atmospheric inversions, Atmos. Chem. Phys., 5, 2691–2702, doi:10.5194/acp-5-2691-2005, 2005.

Butz, A., Guerlet, S., Hasekamp, O., Schepers, D., Galli, A., Aben, I., Frankenberg, C., Hartmann, J. M., Tran, H., Kuze, A., Keppel-Aleks, G., Toon, G., Wunch, D., Wennberg, P., Deutscher, N., Griffith, D., Macatangay, R., Messerschmidt, J., Notholt, J., and Warneke, T.: Toward accurate CO_2 and CH_4 observations from GOSAT, Geophys. Res. Lett., 38, L14812, doi:10.1029/2011GL047888, 2011.

Canadell J. G., Ciais P., Gurney K., Le Quéré C., Piao S., Raupach M. R., and Sabine C. L.: An international effort to quantify regional carbon fluxes, EOS, 92, 81–82, 2011.

Chevallier, F., Maksyutov, S., Bousquet, P., Bréon, F.-M., Saito, R., Yoshida, Y., and Yokota, T.: On the accuracy of the CO_2 surface fluxes to be estimated from the GOSAT observations, Geophys. Res. Lett., 36, L19807, doi:10.1029/2009GL040108, 2009.

Connor, B. J., Bösch, H., Toon, G., Sen, B., Miller, C., and Crisp, D.: Orbiting Carbon Observatory: inverse method and prospective error analysis, J. Geophys. Res., 113, D05305, doi:10.1029/2006JD008336, 2008.

Dee, D. P., Uppala, S. M., Simmons, A. J., Berrisford, P., Poli, P., Kobayashi, S., Andrae, U., Balmaseda, M. A., Balsamo, G., Bauer, P., Bechtold, P., Beljaars, A. C. M., van de Berg,

ACPD
12, 29235–29288, 2012

L., Bidlot, J., Bormann, N., Delsol, C., Dragani, R., Fuentes, M., Geer, A. J., Haimberger, L., Healy, S. B., Hersbach, H., Holm, E. V., Isaksen, L., Kallberg, P., Kohler, M., Matricardi, M., McNally, A. P., Monge-Sanz, B. M., Morcrette, J.-J., Park, B.-K., Peubey, C., de Rosnay, P., Tavolato, C., Thepaut, J.-N., and Vitart, F.: The ERA-Interim reanalysis: configuration and performance of the data assimilation system, Q. J. Roy. Meteorol. Soc., 137, 553–597, 2011.

Deutscher, N. M., Griffith, D. W. T., Bryant, G. W., Wennberg, P. O., Toon, G. C., Washenfelder, R. A., Keppel-Aleks, G., Wunch, D., Yavin, Y., Allen, N. T., Blavier, J.-F., Jiménez, R., Daube, B. C., Bright, A. V., Matross, D. M., Wofsy, S. C., and Park, S.: Total column CO_2 measurements at Darwin, Australia – site description and calibration against in situ aircraft profiles, Atmos. Meas. Tech., 3, 947–958, doi:10.5194/amt-3-947-2010, 2010.

Dolman, A. J., Shvidenko, A., Schepaschenko, D., Ciais, P., Tchebakova, N., Chen, T., van der Molen, M. K., Belelli Marchesini, L., Maximov, T. C., Maksyutov, S., and Schulze, E.-D.: An estimate of the terrestrial carbon budget of Russia using inventory based, eddy covariance and inversion methods, Biogeosciences Discuss., 9, 6579–6626, doi:10.5194/bgd-9-6579-2012, 2012.

Elvidge, C. D., Baugh, K. E., Dietz, J. B., Bland, T., Sutton, P. C., and Kroehl, H. W.: Radiance calibration of DMSP-OLS low-Light imaging data of human settlements – a new device for portraying the Earth's surface entire, Remote Sens. Environ., 68, 77–88, 1999.

Elvidge, C. D., Ziskin, D., Baugh, K. E., Tuttle, B. T., Ghosh, T., Pack, D. W., Erwin, E. H., and Zhizhin, M.: A fifteen year record of global natural gas flaring derived from satellite data, Energies, 2, 595–622, 2009.

Fan, S., Gloor, M., Mahlman, J., Pacala, S., Sarmiento, J., Takahashi, T., and Tans, P.: A large terrestrial carbon sink in north America implied by atmospheric and oceanic carbon dioxide data and models, Science, 282, 442–446, 1998.

Friedl, M. A., McIver, D. K., Hodges, J. C. F., Zhang, X. Y., Muchoney, D., Strahler, A. H., Woodcock, C. E., Gopal, S., Schneider, A., Cooper, A., Baccini, A., Gao, F., and Schaaf, C.: Global land cover mapping from MODIS: algorithms and early results, Remote. Sens. Environ., 83, 287–302, 2002.

Galarneau, T. J., Hamill, T. M., Dole, R. M., and Perlwitz, J.: A Multiscale analysis of the extreme weather events over western Russia and northern Pakistan during July 2010, Mon. Weather Rev., 140, 1639–1664, 2012.

Giglio, L., Loboda, T., Roy, D. P., Quayle, B., and Justice, C. O.: An active-fire based burned area mapping algorithm for the MODIS sensor, Remote. Sens. Environ., 113, 408–420, 2009.

ACPD
12, 29235–29288, 2012

Giglio, L., Randerson, J. T., van der Werf, G. R., Kasibhatla, P. S., Collatz, G. J., Morton, D. C., and DeFries, R. S.: Assessing variability and long-term trends in burned area by merging multiple satellite fire products, Biogeosciences, 7, 1171–1186, doi:10.5194/bg-7-1171-2010, 2010.

GLOBALVIEW-CO2: Cooperative Atmospheric Data Integration Project-Carbon Dioxide, CD-ROM, NOAA ESRL, Boulder, Colorado, 2010.

GLOBALVIEW-CO2: Cooperative Atmospheric Data Integration Project – Carbon Dioxide, CD-ROM, NOAA ESRL, Boulder, Colorado (also available on Internet via anonymous FTP to ftp.cmdl.noaa.gov, Path: ccg/co2/GLOBALVIEW), 2011.

Gloor, M., Fan, S.-M., Pacala, S., and Sarmiento, J.: Optimal sampling of the atmosphere for purpose of inverse modeling: A model study, Global Biogeochem. Cy., 14, 407–428, doi:10.1029/1999GB900052, 2000.

Gloor, M., Gatti, L., Brienen, R. J. W., Feldpausch, T., Phillips, O., Miller, J., Ometto, J.-P., Ribeiro da Rocha, H., Baker, T., Houghton, R., Malhi, Y., Aragão, L., Guyot, J.-L., Zhao, K., Jackson, R., Peylin, P., Sitch, S., Poulter, B., Lomas, M., Zaehle, S., Huntingford, C., and Lloyd, J.: The carbon balance of South America: status, decadal trends and main determinants, Biogeosciences Discuss., 9, 627–671, doi:10.5194/bgd-9-627-2012, 2012.

Grant, R. F., Hutyra, L. R., de Oliveira, R. C., Munger, J. W., Saleska, S. R., and Wofsy, S. C.: Modelling the carbon balance of Amazonian rainforests: resolving ecological controls on net ecosystem productivity, Ecol. Appl., 79, 445–463, 2009.

Gruber, N., Gloor, M., Fletcher, S. E. M., Doney, S. C., Dutkiewicz, S., Follows, M. J., Gerber, M., Jacobson, A. R., Joos, F., Lindsay, K., Menemenlis, D., Mouchet, A., Müller, S. A., Sarmiento, J. L., and Takahashi, T.: Oceanic sources, sinks and transport of atmospheric CO_2, Global Biogeochem. Cy., 23, GB1005, doi:10.1029/2008GB003349, 2009.

Gurney, K. R., Law, R. M., Denning, A. S., Rayner, P. J., Baker, D., Bousquet, P., Bruhwiler, L., Chen, Y.-H., Ciais, P., Fan, S., Fung, I. Y., Gloor, M., Heimann, M., Higuchi, K., John, J., Maki, T., Maksyutov, S., Masarie, K., Peylin, P., Prather, M., Pak, B. C., Randerson, J., Sarmiento, J., Taguchi, S., Takahashi, T., and Yuen, C.-W.: Towards robust regional estimates of CO_2 sources and sinks using atmospheric transport models, Nature, 415, 626–630, 2002.

Gurney, K. R., Law, R. M., Denning, A. S., Rayner, P. J., Pak, B., and Transom-3-L2 modelers: Transcom-3 inversion intercomparison: control results for the estimation of seasonal carbon sources and sinks, Global Biogeochem. Cy., 18, GB1010, doi:10.1029/2003GB002111, 2004.

ACPD

12, 29235–29288, 2012

Gurney, K. R., Chen, Y.-H., Maki, T., Kawa, S. R., Andrews, A., and Zhu, Z.: Sensitivity of atmospheric CO_2 inversions to seasonal and interannual variations in fossil fuel emissions, J. Geophys. Res., 110, D10308, doi:10.1029/2004JD005373, 2005.

Gurney, K. R., Mendoza, D., Zhou, Y., Fischer, M., de la Rue du Can, S., Geethakumar, S., and Miller, C. C.: The Vulcan Project: High resolution fossil fuel combustion CO_2 emissions fluxes for the United States, Environ. Sci. Technol., 43, 5535–5541, 2009.

Hack, J. J, Boville, B. A., Briegleb, B. P., Kiehl, J. T., Rasch, P. J., and Williamson, D. L.: Description of the NCAR community climate model (CCM2), NCAR/TN-382, 108, 1993.

Heimann, M. and Keeling, C.: A three-dimensional model of atmospheric CO_2 transport based on observed winds: 2: Model description and simulated tracer experiments, Geophys. Mon., 55, 237–275, 1989.

Ikeda, M. and Sasai, Y.: Reconstruction of subsurface DIC and alkalinity fields in the North Pacific using assimilation of upper ocean data, Mar. Chem., 72, 343–358, 2000.

Ito, A.: Changing ecophysiological processes and carbon budget in East Asian ecosystems under near-future changes in climate: Implications for long-term monitoring from a process-based model, J. Plant Res., 123, 577–588, 2010.

Jones, P. D. and Briffa, K. R.: Global surface air temperature variations during the twentieth century: Part 1, Spatial, Temporal and Seasonal Details, The Holocene, 2, 165–179, 1992.

Justice, C. O., Giglio, L., Korontzi, S., Owens, J., Morisette, J. T., Roy, D. P., Descloitres, J., Alleaume, S., Petitcolin, F., and Kaufman, Y.: The MODIS fire products, Remote. Sens. Environ., 83, 244–262, 2002.

Kadygrov, N., Maksyutov, S., Eguchi, N., Aoki, T., Nakazawa, T., Yokota, T., and Inoue, G.: Role of simulated GOSAT total column CO_2 observations in surface CO_2 flux uncertainty reduction, J. Geophys. Res., 114, D21208, doi:10.1029/2008JD011597, 2009.

Keeling, C. D., Whorf, T. P., Wahlen, M., and van der Plicht, J.: Interannual extremes in the rate of rise of atmospheric carbon dioxide since 1980, Nature, 375, 666–670, 1995.

Kindermann, G. E., McCallum, I., Fritz, S., and Obersteiner, M.: A global forest growing stock, biomass and carbon map based on FAO statistics, Silva Fennica, 42, 387–396, 2008.

Koyama, Y., Maksyutov, S., and Valsala, V.: Model analysis of observational data of the atmospheric tracers for the estimation of greenhouse gases in East Asia, Global Environment Research Account for National Institutes in FY2008, Ministry of the Environment, Japan, 49–95, 2009.

ACPD
12, 29235–29288, 2012

Kuze, A., Suto, H., Nakajima, M., and Hamazaki, T.: Thermal and near infrared sensor for carbon observation Fourier-transform spectrometer on the Greenhouse Gases Observing Satellite for greenhouse gases monitoring, Appl. Opt., 48, 6716–6733, 2009.

McKinley, G. A., Follows, M. J., and Marshall, J.: Mechanism of air–sea CO_2 flux variability in the equatorial Pacific and North Atlantic, Global Biogeochem. Cy., 18, GB2011, doi:10.1029/2003GB002179, 2004.

Maksyutov, S., Patra, P. K., Onishi, R., Saeki, T., and Nakazawa, T.: NIES/FRCGC global atmospheric tracer transport model: description, validation, and surface sources and sinks inversion, J. Earth Simulator, 9, 3–18, 2008.

Melillo, J. M., Steudler, P. A., Aber, J. D., Newkirk, K., Lux, H., Bowles, F. P., Catricala, C., Magill, A., Ahrens, T., and Morrisseau, S.: Soil Warming and Carbon-Cycle Feedbacks to the Climate System, Science, 298, 2173–2176, 2002.

Messerschmidt, J., Macatangay, R., Notholt, J., Petri, C., Warneke, T., and Weinzierl, C.: Side by side measurements of CO_2 by ground-based Fourier transform spectrometry (FTS), Tellus B, 62, 749–758, 2010.

Messerschmidt, J., Chen, H., Deutscher, N. M., Gerbig, C., Grupe, P., Katrynski, K., Koch, F.-T., Lavric, J. V., Notholt, J., Rödenbeck, C., Ruhe, W., Warneke, T., and Weinzierl, C.: Automated ground-based remote sensing measurements of greenhouse gases at the Bialystok site in comparison with collocated in situ measurements and model data, Atmos. Chem. Phys., 12, 6741–6755, doi:10.5194/acp-12-6741-2012, 2012.

Monsi, M. and Saeki, T.: Uber den Lichtfaktor in den Pflanzengesellschaften und seine Bedeutung für die Stoffproduktion, Jpn. J. Bot., 14, 22–52, 1953.

Morino, I., Uchino, O., Inoue, M., Yoshida, Y., Yokota, T., Wennberg, P. O., Toon, G. C., Wunch, D., Roehl, C. M., Notholt, J., Warneke, T., Messerschmidt, J., Griffith, D. W. T., Deutscher, N. M., Sherlock, V., Connor, B., Robinson, J., Sussmann, R., and Rettinger, M.: Preliminary validation of column-averaged volume mixing ratios of carbon dioxide and methane retrieved from GOSAT short-wavelength infrared spectra, Atmos. Meas. Tech., 4, 1061–1076, doi:10.5194/amt-4-1061-2011, 2011.

Niwa, Y., Patra, P. K., Sawa, Y., Machida, T., Matsueda, H., Belikov, D., Maki, T., Ikegami, M., Imasu, R., Maksyutov, S., Oda, T., Satoh, M., and Takigawa, M.: Three-dimensional variations of atmospheric CO_2: aircraft measurements and multi-transport model simulations, Atmos. Chem. Phys., 11, 13359–13375, doi:10.5194/acp-11-13359-2011, 2011.

ACPD
12, 29235–29288, 2012

Oda, T. and Maksyutov, S.: A very high-resolution (1 km×1 km) global fossil fuel CO_2 emission inventory derived using a point source database and satellite observations of nighttime lights, Atmos. Chem. Phys., 11, 543–556, doi:10.5194/acp-11-543-2011, 2011.

Oda, T., Miller, J. B., Maksyutov, S., Andres, R. J., and Elvidge, C. D.: Two fossil fuel CO_2 emissions datasets used for CarbonTracker, Atmos. Chem. Phys., in preparation, 2012.

O'Dell, C. W., Connor, B., Bösch, H., O'Brien, D., Frankenberg, C., Castano, R., Christi, M., Eldering, D., Fisher, B., Gunson, M., McDuffie, J., Miller, C. E., Natraj, V., Oyafuso, F., Polonsky, I., Smyth, M., Taylor, T., Toon, G. C., Wennberg, P. O., and Wunch, D.: The ACOS CO_2 retrieval algorithm – Part 1: Description and validation against synthetic observations, Atmos. Meas. Tech., 5, 99–121, doi:10.5194/amt-5-99-2012, 2012.

Ohyama, H., Morino, I., Nagahama, T., Machida, T., Suto, H., Oguma, H., Sawa, Y., Matsueda, H., Sugimoto, N., Nakane, H., and Nakagawa, K.: Column-averaged volume mixing ratio of CO_2 measured with ground-based Fourier transform spectrometer at Tsukuba, J. Geophys. Res., 114, D18303, doi:10.1029/2008JD011465, 2009.

Olson, R. J., Johnson, K. R., Zheng, D. L., and Scurlock, J. M. O.: Global and Regional Ecosystem Modeling: Databases of Model Drivers and Validation Measurements, Oak Ridge National Laboratory, 2001.

Onogi, K., Tsutsui, J., Koide, H., Sakamoto, M., Kobayashi, S., Hatsushika, H., Matsumoto, T., Yamazaki, N., Kamahori, H., Takahashi, K., Kadokura, S., Wada, K., Kato, K., Oyama, R., Ose, T., Mannoji, N., and Taira, R.: The JRA-25 Reanalysis, J. Meteorol. Soc. Jap., 85, 369–432, 2007.

Orr, J. C., Najjar, R., Sabine, C. L., and Joos, F.: Abiotic-HOWTO, LSCE/CEA Saclay, Gif-sur-Yvette, France, 25 pp., 1999.

Oshchepkov, S., Bril, A., Yokota, T., Morino, I., Yoshida, Y., Matsunaga, T., Belikov, D., Wunch, D., Wennberg, P., Toon, G., O'Dell, C., Butz, A., Guerlet, S., Cogan, A., Bösch, H., Eguchi, N., Deutscher, N., Griffith, D., Macatangay, R., Notholt, J., Sussmann, R., Rettinger, M., Sherlock, V., Robinson, J., Kyrö, E., Heikkinen, P., Feist, D. G., Nagahama, T., Kadygrov, N., Maksyutov, S., Uchino, O., and Watanabe, H.: Effects of atmospheric light scattering on spectroscopic observations of greenhouse gases from space: Validation of PPDF-based CO_2 retrievals from GOSAT, J. Geophys. Res., 117, D12305, doi:10.1029/2012JD017505, 2012.

Pacala, S. W., Hurtt, G., Baker, D., Peylin, P., Houghton, R. A., Birdsey, R. A., Heath, L., Sundquist, E. T., Stallard, R. F., Ciais, P., Moorcroft, P., Caspersen, J. P., Shevliakova, E.,

ACPD
12, 29235–29288, 2012

Moore, B., Kohlmaier, G., Holland, E., Gloor, M., Harmon, M. E., Fan, S. M., Sarmiento, J. L., Goodale, C. L., Schimel, D., and Field, C. B.: Consistent land- and atmosphere-based U.S. carbon sink estimates, Science, 292, 2316–2320, 2001.

Patra, P. K., Ishizawa, M., Maksyutov, S., Nakazawa, T., and Inoue, G.: Role of biomass burning and climate anomalies for land-atmosphere carbon fluxes based on inverse modeling of atmospheric CO_2, Global Biogeochem. Cycles, 19, GB3005, doi:10.1029/2004GB002258, 2005a.

Patra, P. K., Maksyutov, S., and Nakazawa, T.: Analysis of atmospheric CO_2 growth rates at Mauna Loa using inverse model derived CO_2 fluxes, Tellus, 57B, 357–365, 2005b.

Patra, P. K., Houweling, S., Krol, M., Bousquet, P., Belikov, D., Bergmann, D., Bian, H., Cameron-Smith, P., Chipperfield, M. P., Corbin, K., Fortems-Cheiney, A., Fraser, A., Gloor, E., Hess, P., Ito, A., Kawa, S. R., Law, R. M., Loh, Z., Maksyutov, S., Meng, L., Palmer, P. I., Prinn, R. G., Rigby, M., Saito, R., and Wilson, C.: TransCom model simulations of CH_4 and related species: linking transport, surface flux and chemical loss with CH_4 variability in the troposphere and lower stratosphere, Atmos. Chem. Phys., 11, 12813–12837, doi:10.5194/acp-11-12813-2011, 2011.

Peters, W., Jacobson, A. R., Sweeney, C., Andrews, A. E., Conway, T. J., Masarie, K., Miller, J. B., Bruhwiler, L. M. P., Petron, G., Hirsch, A. I., Worthy, D. E. J., van der Werf, G. R., Randerson, J. T., Wennberg, P. O., Krol, M. C., and Tans, P. P.: An atmospheric perspective on north American carbon dioxide exchange: CarbonTracker, P. Natl. Acad. Sci., 104, 18925–18930, 2007.

Piao, S., Fang, J., Ciais, P., Peylin, P., Huang, Y., Sitch, S., and Wang, T.: The carbon balance of terrestrial ecosystems in China, Nature, 458, 1009–1013, 2009.

Rayner P. J. and O'Brien, D. M.: The utility of remotely sensed CO_2 concentration data in surface source inversions, Geophys. Res. Lett., 28, 175–178, 2001.

Rayner, P., Enting, I., Francey, R., and Langenfelds, R.: Reconstructing the recent carbon cycle from atmospheric CO_2, $\delta^{13}C$ and O_2/N_2 observations, Tellus, 51B, 213–232, 1999.

Saeki, T., Maksyutov, S., Sasakawa, M., Machida, T., Arshinov, M., Tans, P., Conway, T. J., Saito, M., Valsala, V., Oda, T., and Andres, R. J.: Carbon flux estimation for Siberia by inverse modeling constrained by aircraft and tower CO_2 measurements, J. Geophys. Res., in review, 2012.

Saito, M., Ito, A., and Maksyutov, S.: Evaluation of biases in JRA-25/JCDAS precipitation and their impact on the global terrestrial carbon balance, J. Climate, 24, 4109–4125, 2011.

ACPD
12, 29235–29288, 2012

Saito, M., Ito, A., and Maksyutov, S.: Synthesis modeling of atmospheric CO_2 variability and terrestrial biomass with inversion scheme, Global Biogeochem. Cy., in preparation, 2013.

Saito, R., Houweling, S., Patra, P. K., Belikov, D., Lokupitiya, R., Niwa, Y., Chevallier, F., Saeki, T., and Maksyutov, S.: TransCom satellite intercomparison experiment: Construction of a bias corrected atmospheric CO_2 climatology, J. Geophys. Res., 116, D21120, doi:10.1029/2011JD016033, 2011.

Scurlock, J. M. O., Cramer, W., Olson, R. J., Parton, W. J., and Prince, S. D.: Terrestrial NPP: toward a consistent data set for global model evaluation, Ecol. Appl., 9, 913–919, 1999.

Shvidenko A. Z., Shchepashchenko, D. G., Vaganov, E. A., Sukhinin, A. I., Maksyutov, S., McCallum, I., and Lakyda, I. P.: Impact of Wildfire in Russia between 1998–2010 on Ecosystems and the Global Carbon Budget, Dokl. Earth Sci., 441, 1678–1682, 2011.

Stephens, B. B., Gurney, K. R., Tans, P. P., Sweeney, C., Peters, W., Bruhwiler, L., Ciais, P., Ramonet, M., Bousquet, P., Nakazawa, T., Aoki, S., Machida, T., Inoue, G., Vinnichenko, N., Lloyd, J., Jordan, A., Heimann, M., Shibistova, O., Langenfelds, R. L., Steele, L. P., Francey, R. J., and Denning, A. S.: Weak northern and strong tropical land carbon uptake from vertical profiles of atmospheric CO_2, Science, 316, 1732–1735, 2007.

Takahashi, T., Sutherland, S. C., and Kozyr, A.: Global ocean surface water partial pressure of CO_2 database: measurements performed during 1968-2006 (Version 1.0). ORNL/CDIAC-152, NDP-08, Carbon Dioxide Information Analysis Center, 2007.

Takahashi, T., Sutherland, S. C., Wanninkhof, R., Sweeney, C., Feely, R. A., Chipman, D. W., Hales, B., Friederich, G., Chavez, F., Sabine, C., Watson, A., Bakker, D. C. E., Schuster, U., Metzl, N., Yoshikawa-Inoue, H., Ishii, M., Midorikawa, T., Nojiri, Y., Kartzinger, A., Steinhoff, T., Hoppema, M., Olafsson, J., Arnarson, T. S., Tilbrook, B., Johannessen, T., Olsen, A., Bellerby, R., Wong, C. S., Delille, B., Bates, N. R., and de Baar, H. J. W.: Climatological mean and decadal changes in surface ocean pCO_2 and net sea-air CO_2 flux over the global oceans, Deep-Sea Res. II, 56, 554–577, 2009.

Takagi H., Saeki, T., Oda, T., Saito, M., Valsala, V., Belikov, D., Saito, R., Yoshida, Y., Morino, I., Uchino, O., Andres, R. J., Yokota, T., and Maksyutov, S.: On the benefit of GOSAT observations to the estimation of regional CO_2 fluxes, SOLA, 7, 161–164, 2011.

Tans, P. P., Fung, I. Y., and Takahashi, T.: Observational constrains on the global atmospheric CO_2 budget, Science, 247, 1431–1438, 1990.

Tarantola, A.: Inverse Problem Theory and Methods for Model Parameter Estimation, Society for Industrial and Applied Mathematics, Philadelphia, USA, 342 pp., 2005.

ACPD
12, 29235–29288, 2012

Tiedtke, M.: A comprehensive mass flux scheme for cumulus parameterization in large scale models, Mon. Weather Rev., 117, 1779–1800, 1989.
Uchino, O., Kikuchi, N., Sakai, T., Morino, I., Yoshida, Y., Nagai, T., Shimizu, A., Shibata, T., Yamazaki, A., Uchiyama, A., Kikuchi, N., Oshchepkov, S., Bril, A., and Yokota, T.: Influence of aerosols and thin cirrus clouds on the GOSAT-observed CO_2: a case study over Tsukuba, Atmos. Chem. Phys., 12, 3393–3404, doi:10.5194/acp-12-3393-2012, 2012.
Valsala, V. and Maksyutov, S.: Simulation and assimilation of global ocean pCO_2 and air-sea CO_2 fluxes using ship observations of surface ocean pCO_2 in a simplified biogeochemical offline model, Tellus-B, 62B, 821–840, 2010.
Valsala, V., Maksyutov, S., and Ikeda, M.: Design and validation of an offline Oceanic Tracer Transport Model for Carbon Cycle study, J. Climate, 21, 2752–2769, 2008.
Vermote, E. F., El Saleous, N. Z., and Justice, C. O.: Operational atmospheric correction of the MODIS data in the visible to middle infrared: First results, Remote. Sens. Environ., 83, 97–111, 2002.
Washenfelder, R. A., Toon, G. C., Blavier, J.-F., Yang, Z., Allen, N. T., Wennberg, P. O., Vay, S. A., Matross, D. M., and Daube, B. C.: Carbon dioxide column abundances at the Wisconsin Tall Tower site, J. Geophys. Res., 111, D22305, doi:10.1029/2006JD007154, 2006.
Weaver, C. J., Douglass, A. R., and Rood, R. B.: Thermodynamic balance of three-dimensional stratospheric winds derived from a data assimilation procedure, J. Atmos. Sci., 50, 2987–2993, 1993.
van der Werf, G. R., Randerson, J. T., Giglio, L., Collatz, G. J., Mu, M., Kasibhatla, P. S., Morton, D. C., DeFries, R. S., Jin, Y., and van Leeuwen, T. T.: Global fire emissions and the contribution of deforestation, savanna, forest, agricultural, and peat fires (1997–2009), Atmos. Chem. Phys., 10, 11707–11735, doi:10.5194/acp-10-11707-2010, 2010.
Wunch, D., Toon, G. C., Blavier, J.-F. L., Washenfelder, R. A., Notholt, J., Connor, B. J., Griffith, D. W. T., Sherlock, V., and Wennberg, P. O.: The Total Carbon Column Observing Network, Philos. Trans. R. Soc. A, 369, 1943, 2087–2112, doi:10.1098/rsta.2010.0240, 2011.
Yokota, T., Yoshida, Y., Eguchi, N., Ota, Y., Tanaka, T., Watanabe, H., and Maksyutov, S.: Global concentrations of CO_2 and CH_4 retrieved from GOSAT: First preliminary results, SOLA, 5, 160–163, doi:10.2151/sola.2009-041, 2009.
Yoshida, Y., Oguma, H., Morino, I., Suto, H., Kuze, A., and Yokota, T.: Mountaintop observation of CO_2 absorption spectra using a short wavelength infrared Fourier transform spectrometer, Appl. Optics, 49, 71–79, 2009.

ACPD
12, 29235–29288, 2012

Yoshida, Y., Ota, Y., Eguchi, N., Kikuchi, N., Nobuta, K., Tran, H., Morino, I., and Yokota, T.: Retrieval algorithm for CO_2 and CH_4 column abundances from short-wavelength infrared spectral observations by the Greenhouse gases observing satellite, Atmos. Meas. Tech., 4, 717–734, doi:10.5194/amt-4-717-2011, 2011.

Yoshida, Y., Kikuchi, N., and Yokota, T.: On-orbit radiometric calibration of SWIR bands of TANSO-FTS onboard GOSAT, Atmos. Meas. Tech., 5, 2515–2523, doi:10.5194/amt-5-2515-2012, 2012.

Yoshida, Y., Kikuchi, N., Morino, I., Uchino, O., Oshchepkov, S., Bril, A., Saeki, T., Schutgens, N., Toon, G. C., Wunch, D., Roehl, C. M., Wennberg, P. O., Griffith, D. W. T., Deutscher, N. M., Warneke, T., Notholt, J., Robinson, J., Sherlock, V., Connor, B., Rettinger, M., Sussmann, R., Ahonen, P., Heikkinen, P., Kyrö, E., and Yokota, T.: Improvement of the retrieval algorithm for GOSAT SWIR XCO_2 and XCH_4 and their validation using TCCON data, Atmos. Meas. Tech., in preparation, 2013.

Ziskin, D., Baugh, K., Hsu F.C., Ghosh, T., and Elvidge, C.: Methods used for the 2006 radiance lights, Proc. 30th Asia-Pacific Advanced Network Meeting, 131–142, 2010.

ACPD

12, 29235–29288, 2012

Table 1. Root mean square differences (RMS difference) between TCCON and modeled concentrations (in ppm) over one year between June 2009 and May 2010. Also listed is the RMS of TCCON observation uncertainty (TCCON uncertainty in ppm).

SITE	LAT	LON	TCCON uncertainty	RMS difference
Bialystok, Poland	53.23	23.03	0.91	1.05
Bremen, Germany	53.10	8.85	0.90	1.28
Darwin, Australia	−12.43	130.89	0.44	0.33
Garmisch, Germany	47.48	11.06	1.32	1.49
Izana, Tenerife	28.30	−16.48	0.43	0.94
Lamont, USA	36.60	−97.49	1.27	0.36
Lauder, New Zealand	−45.04	169.68	1.07	0.42
Ny_Alesund, Spitsbergen	78.92	11.92	1.58	1.24
Orleans, Franc	47.97	2.11	0.69	0.75
Park Falls, USA	45.94	−90.27	1.01	0.67
Sodankyla, Finland	67.37	26.63	0.62	1.05
Tsukuba, Japan	36.05	140.12	1.96	0.60
Wollongong, Australia	−34.41	150.88	0.77	0.50

ACPD
12, 29235–29288, 2012

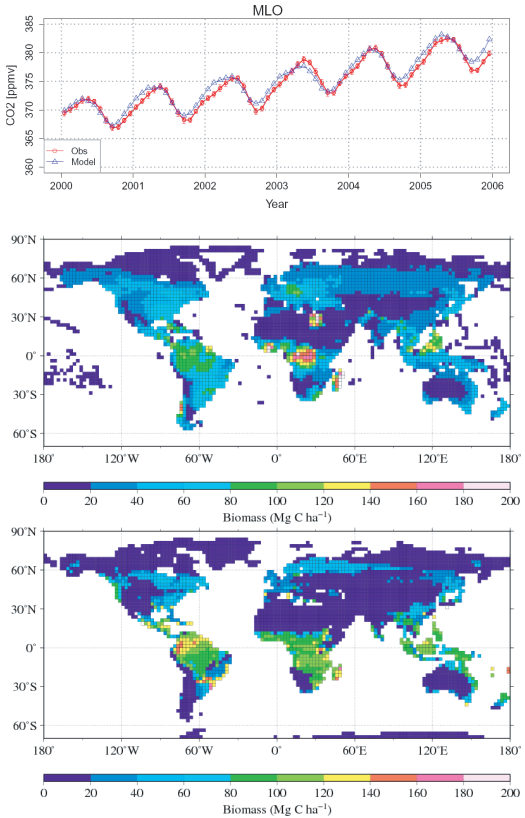

Fig. 1. Comparison of the optimized VISIT model results to the observations. Top: forward simulation of atmospheric CO_2 (ppm) at Mauna-Loa (red circles), and Globalview (blue triangles). Below: global map of gridded mean biomass (Mg C ha^{-1}): (middle) IIASA database, (bottom) optimized VISIT.

ACPD
12, 29235–29288, 2012

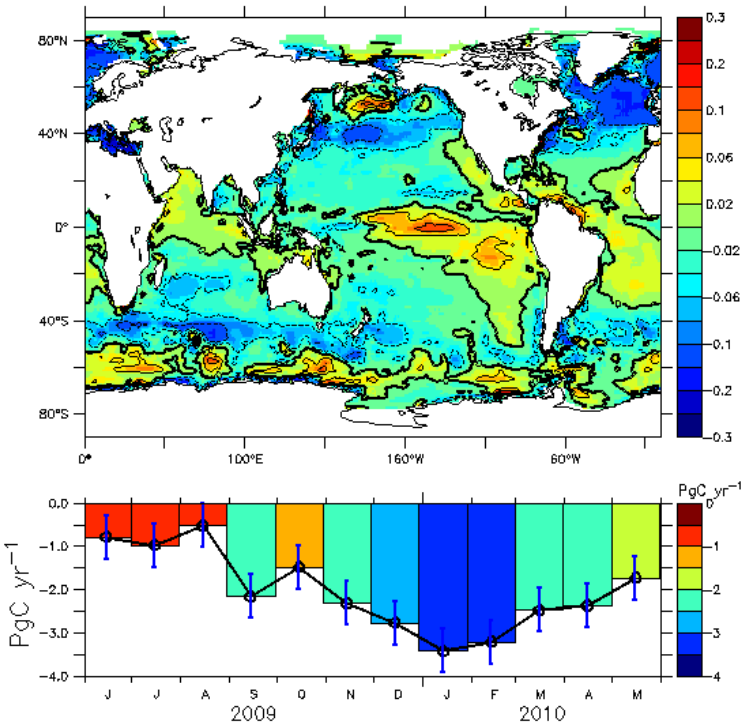

Fig. 2. Top: June 2009 to May 2010 averaged air-to-sea CO_2 prior fluxes (gC m^{-2} day^{-1}) used in the inversion. Bottom: global integral of air-to-sea CO_2 fluxes (PgC yr^{-1}) and corresponding global mean data uncertainties used in the inversion.

ACPD
12, 29235–29288, 2012

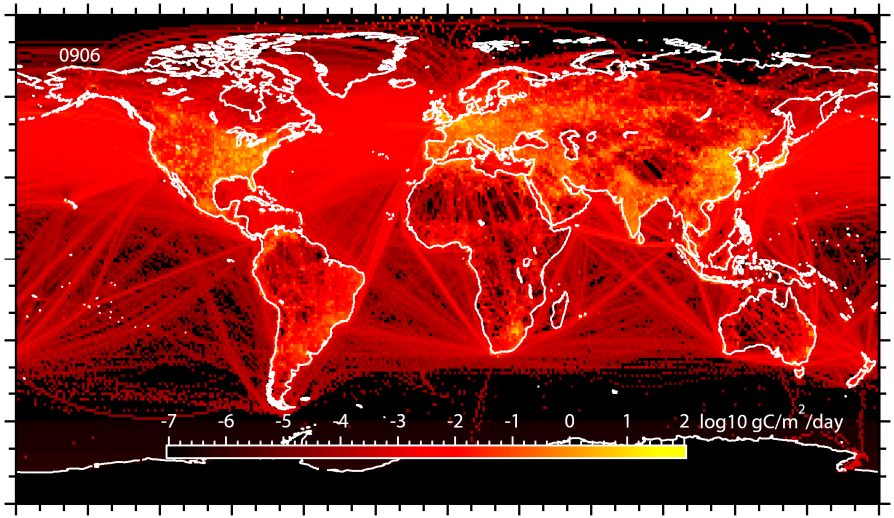

Fig. 3. Global distribution of the annual mean CO_2 emissions due to burning fossil fuels.

ACPD
12, 29235–29288, 2012

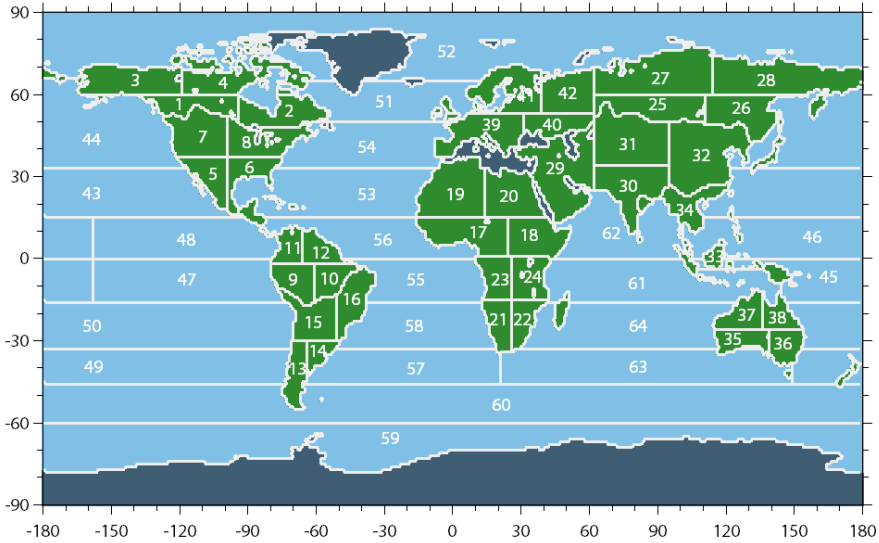

Fig. 4. Boundaries of the 64 source regions adopted in this study. The numbers on the figure are the region IDs of each region. Regions shaded with dark blue are not considered in the flux estimation.

ACPD
12, 29235–29288, 2012

Regional CO_2 flux estimates for 2009–2010

S. Maksyutov et al.

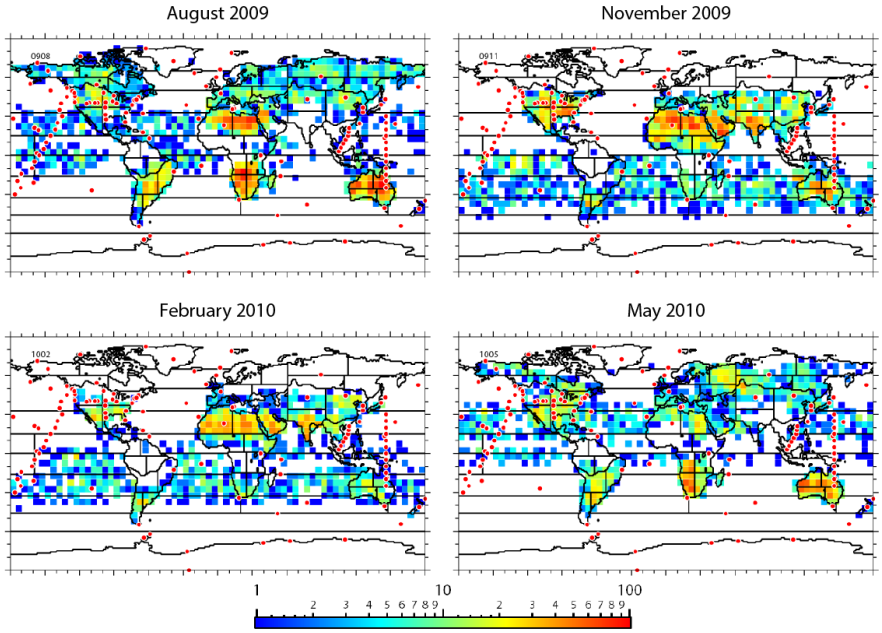

Fig. 5. The number of GOSAT Level 2 X_{CO_2} data records per each of $5^{\circ} \times 5^{\circ}$ grid cells during the months of August 2009, November 2009, February 2010, and May 2010. Red circles indicate the locations of the GV measurement sites chosen for this study.

ACPD
12, 29235–29288, 2012

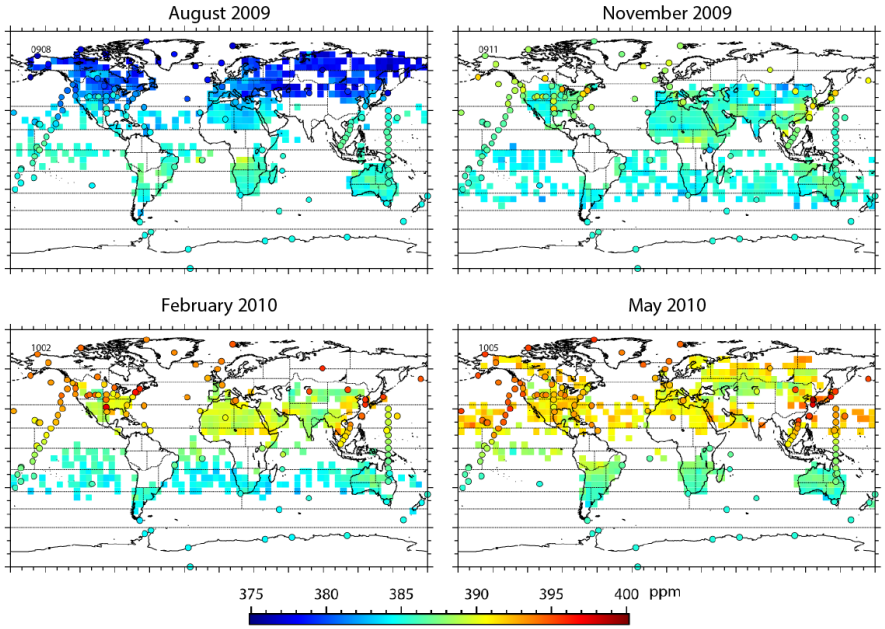

Fig. 6. Version 02.00 of the X_{CO_2} retrievals in the form of input to our inverse modeling scheme (gridded to $5^\circ \times 5^\circ$ cells and averaged on a monthly time scale). Cells with three or more retrievals per month are shown here. The bias was corrected by raising each X_{CO_2} retrieval by 1.20 ppm. Overlaid are GLOBALVIEW values (in circles) that are also in the form of input to inverse modeling (monthly means). Values for the months of August 2009 (summer in the Northern Hemisphere), November 2009 (fall), February 2010 (winter), and May 2010 (spring) are shown.

ACPD
12, 29235–29288, 2012

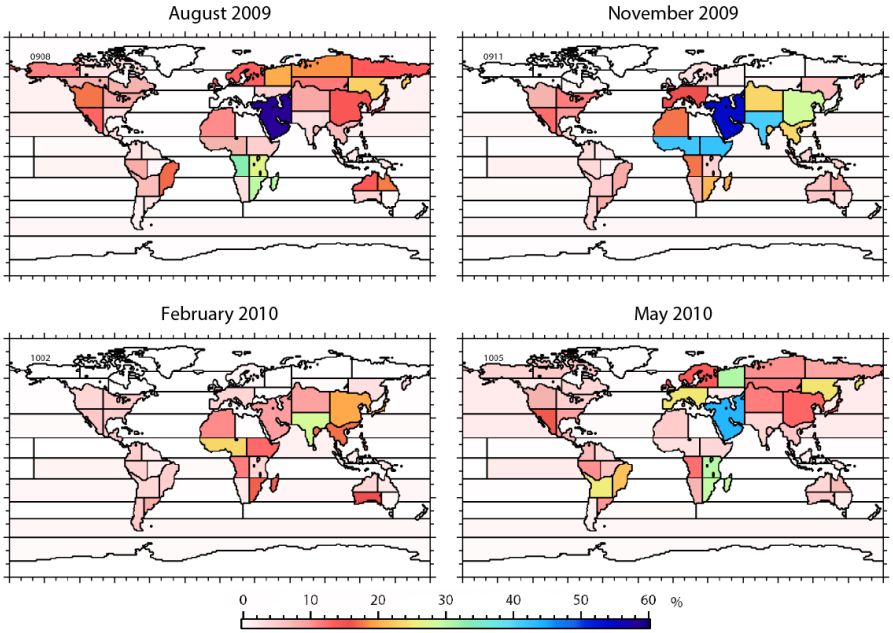

Fig. 7. Percent reduction in the uncertainty of monthly surface flux estimates, attained by adding the GOSAT X_{CO_2} retrievals to the GLOBALVIEW dataset.

ACPD
12, 29235–29288, 2012

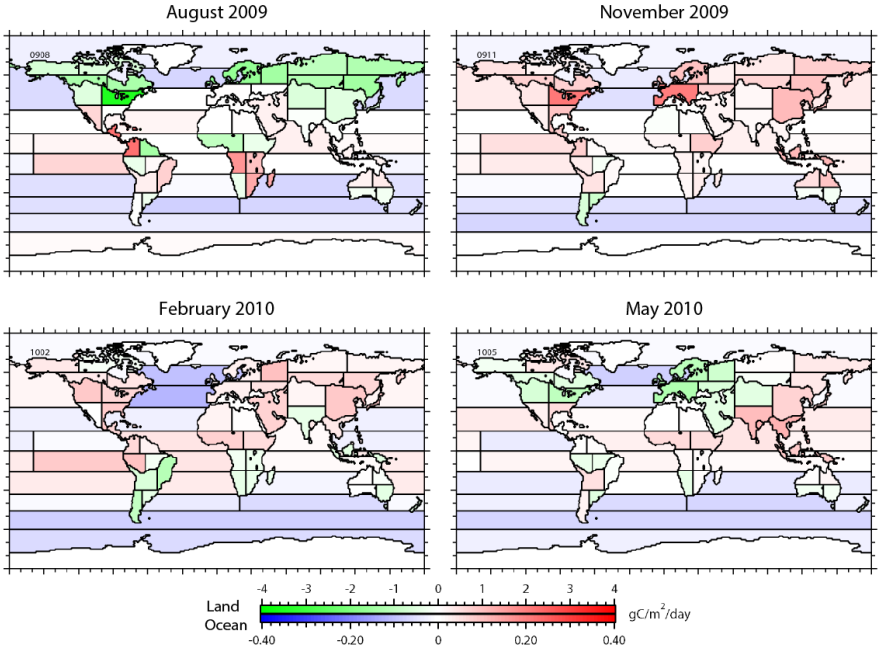

Fig. 8. Monthly fluxes (gC m^{-2} day^{-1}) estimated for the 64 subcontinental regions using GV observations and GOSAT X_{CO_2} retrievals, for the months of August 2009 (summer in the Northern Hemisphere), November 2009 (fall), February 2010 (winter), and May 2010 (spring). Note the different color-coded scales for land and ocean regions.

ACPD
12, 29235–29288, 2012

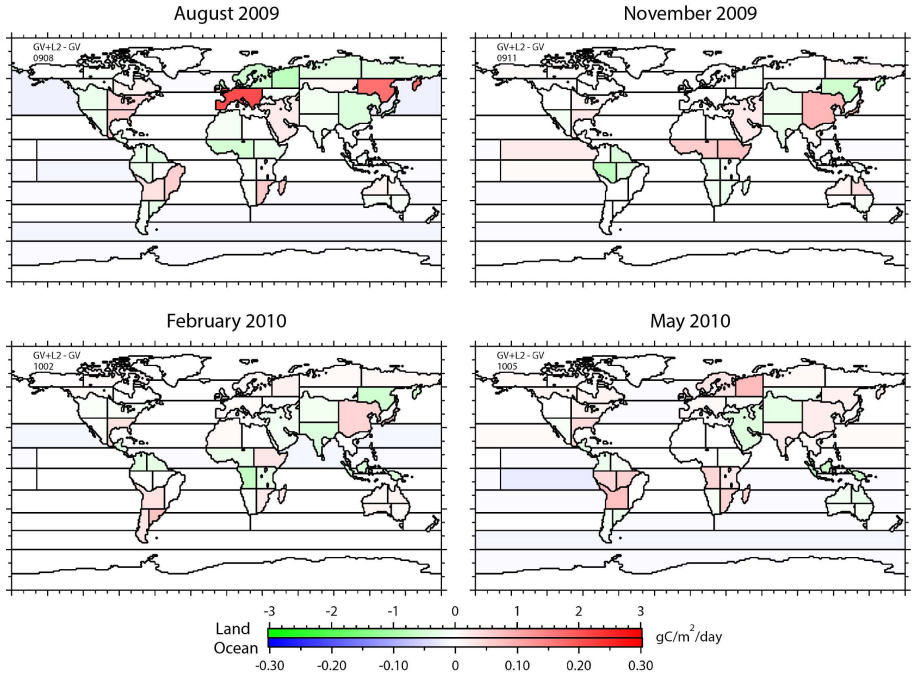

Fig. 9. Differences between the fluxes estimated from GV observations only and those from combined GV and GOSAT X_{CO_2} retrievals. Note the different color-coded scales for land and ocean regions.

ACPD
12, 29235–29288, 2012

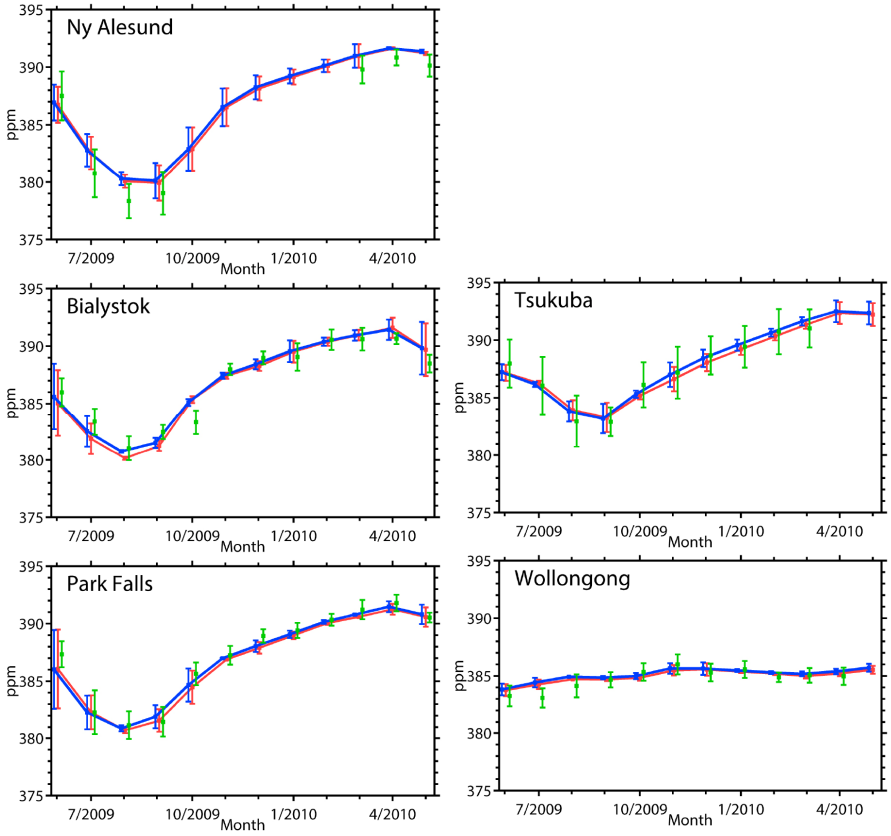

Fig. 10. Time series of data collected at five TCCON sites (in green) and corresponding NIES-TM forward simulation results based on the GV-only a posteriori fluxes (in red), and for combined GV and GOSAT X_{CO_2} retrievals (blues) for sites at: Ny Ålesund, Norway (78.55° N, 11.55° E), Bialystok, Poland (53.23° N, 23.03° E), Park Falls, USA (45.95° N, 90.27° W), Tsukuba, Japan (36.05° N, 140.12° E) and Wollongong, Australia (34.41° S, 150.88° E).

ACPD
12, 29235–29288, 2012

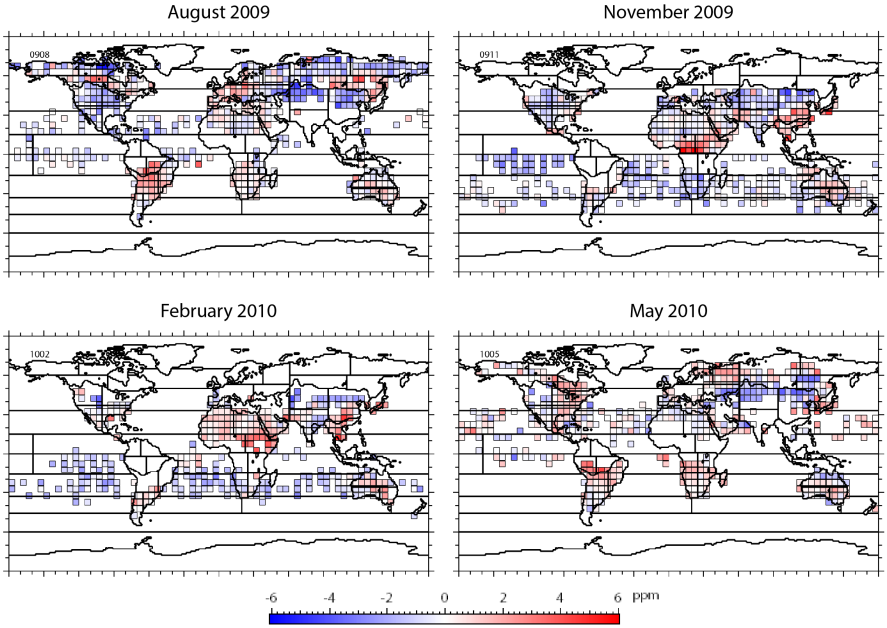

Fig. 11. Monthly mean GOSAT X_{CO_2} retrievals in $5^\circ \times 5^\circ$ grid cells minus the corresponding reference X_{CO_2} concentrations. See text for explanation.

ACPD
12, 29235–29288, 2012

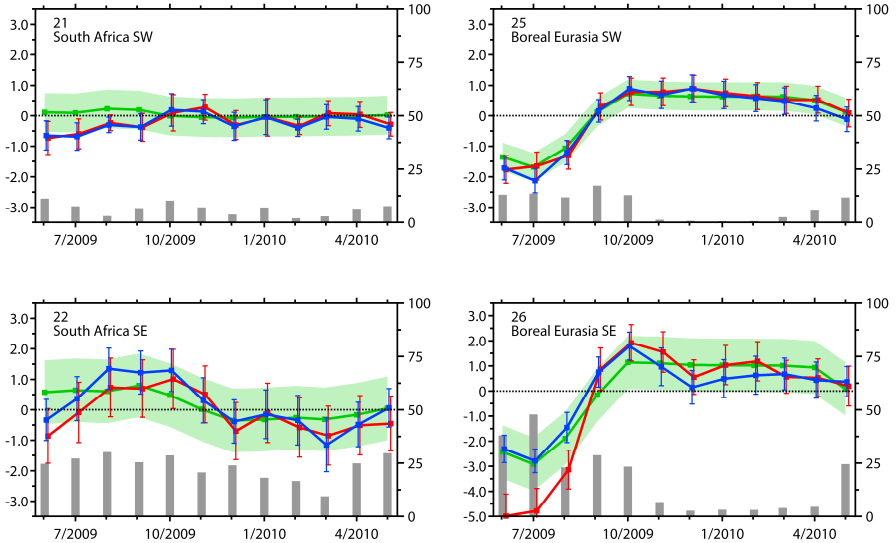

Fig. 12. Time series of regionally averaged fluxes ($gC\,m^{-2}\,day^{-1}$) for June 2009 to May 2010, for quadrants (top to bottom: SW, SE, NW, NE) in the South Africa (left column), boreal Eurasia (right column) subcontinental regions. The graphs show prior fluxes (green lines), estimated fluxes using GV data (red lines), and estimated fluxes using GV and GOSAT data (blue lines). The error bars show flux uncertainties. The gray bars represent the percent reduction in the uncertainty (UR, Eq. 6) (scale on right side of graphs). Estimated flux figures for all 64 regions are available in the Supplement.

ACPD
12, 29235–29288, 2012

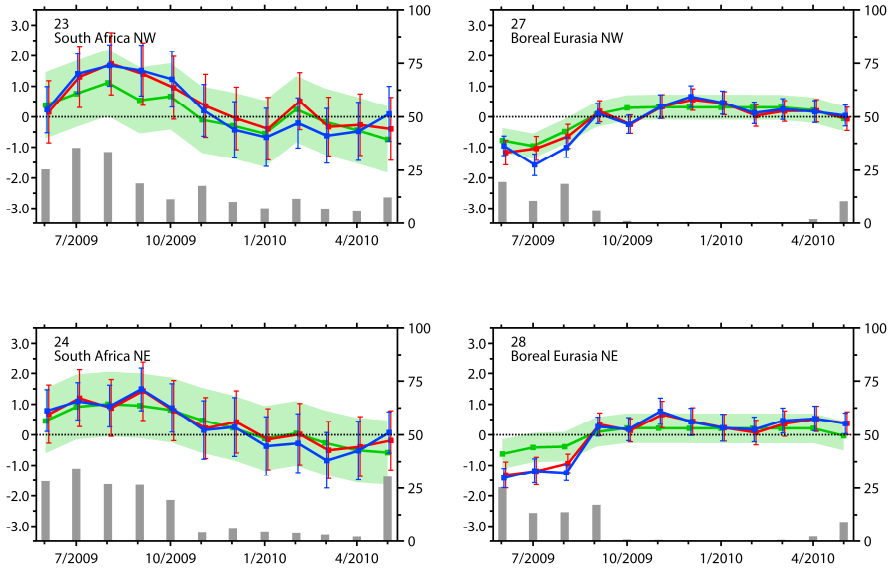

Fig. 12. Continued.

ACPD
12, 29235–29288, 2012

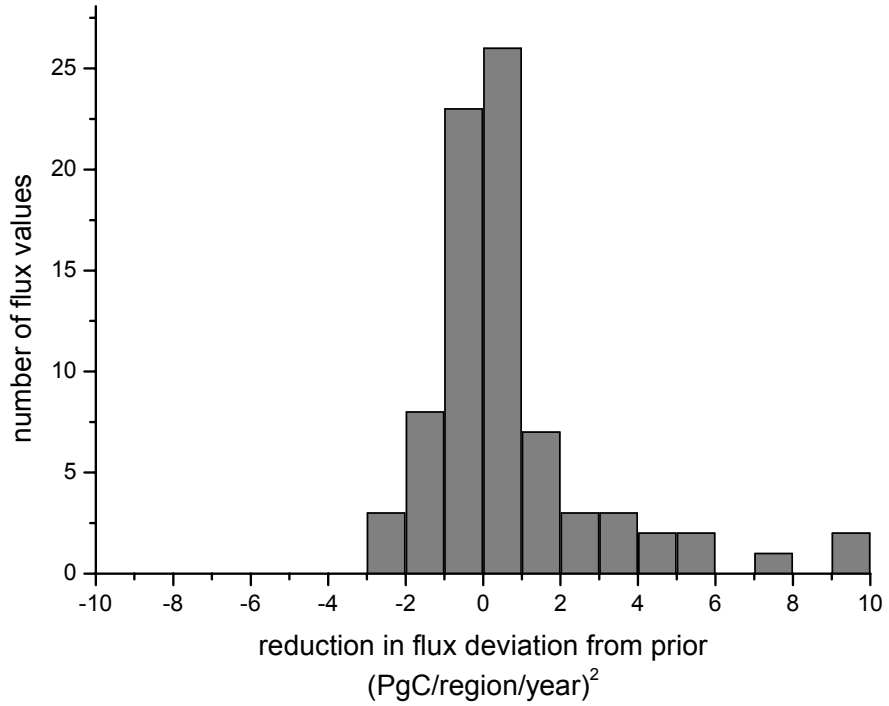

Fig. 13. Reduction in flux deviation from prior due to addition of the GOSAT observations expressed as $\Delta \boldsymbol{m}^2$ (introduced in Eq. 7) in $(\mathrm{PgC/region/year})^2$ for regions and months where reduction in uncertainty is significant (UR > 20 %).

ACPD
12, 29235–29288, 2012